Linear stability analysis in fluid-structure interaction with transpiration. Part II: numerical analysis and applications

Miguel Angel Fernández, Patrick Le Tallec

INRIA

INSTITUT NATIONAL DE RECHERCHE EN INFORMATIQUE ET EN AUTOMATIQUE

Linear stability analysis in fluid-structure interaction with transpiration. Part II: numerical analysis and applications

Miguel-Ángel Fernández — Patrick Le Tallec

N° 4571

Septembre 2002

THÈME 4

ISSN 0249-6399 ISRN INRIA/RR--4571--FR+ENG

Linear stability analysis in fluid-structure interaction with transpiration. Part II: numerical analysis and applications

Miguel-Ángel Fernández*, Patrick Le Tallec†

Thème 4 — Simulation et optimisation
de systèmes complexes
Projet MACS

Rapport de recherche n° 4571 — Septembre 2002 — 66 pages

Abstract: We address the problem of flutter analysis of a coupled fluid-structure system involving an incompressible Newtonian fluid and a reduced structure. We use the *Linearization Principle* approach developed in Part I, particularly suited for fluid-structure problems involving moving boundaries. Thus, the stability analysis is reduced to the computation of the leftmost eigenvalues of a coupled eigenproblem of minimal complexity. The coupling is realized through specific transpiration interface conditions. The eigenproblem is discretized using a finite element approximation and its smallest real part eigenvalues are computed by combining a generalized Cayley transform and an Implicit Restarted Arnoldi Method. The numerical results are compared to former approaches and experimental data. The quality of these numerical results is very satisfactory and promising.

Key-words: Fluid-structure interaction, transpiration, flutter, finite elements, sparse generalized eigenproblems, Cayley transform, Arnoldi's method.

* INRIA-MACS. Present address: École Polytechnique Fédérale de Lausanne, IMA, CH-1015, Lausanne, Switzerland, email: miguel.fernandez@epfl.ch

† École Polytechnique, DGAE, F-91128 Palaiseau Cedex, email: patrick.letallec@polytechnique.fr

Unité de recherche INRIA Rocquencourt
Domaine de Voluceau, Rocquencourt, BP 105, 78153 Le Chesnay Cedex (France)
Téléphone : +33 1 39 63 55 11 — Télécopie : +33 1 39 63 53 30

Stabilité linéaire en interaction fluide-structure avec transpiration. Partie II: analyse numérique et applications

Résumé : Dans ce travail on s'intéresse à l'étude du flottement dans un système couplé fluide-structure. Ce système comporte un fluide Newtonien incompressible et une structure réduite. On utilise l'approche du *Principe de Linéarisation* développée dans la Partie I et adaptée aux problèmes d'interaction fluide-structure avec des frontières mobiles. Ainsi, l'analyse de stabilité se réduit au calcul des valeurs propres avec plus petite partie réelle d'un problème spectral couplé de complexité minimale. Le couplage est opéré par des conditions de type transpiration sur une interface fixe. Le problème aux valeurs propres est discrétisé par une méthode d'éléments finis. Les valeurs propres de plus petite partie réelle sont approchées en combinant la transformation de Cayley généralisée et une méthode IRAM (Implicit Restarted Arnoldi Method). Les résultats numériques obtenus sont finalement comparés à d'autres approches et résultats expérimentaux.

Mots-clés : Interaction fluide-structure, transpiration, flottement, éléments finis, problème aux valeurs propres généralisé, transformation de Cayley, méthode d'Arnoldi.

1 Introduction

A body immersed in a fluid flow undergoes vibrations which can modify its geometry. Indeed, if a fluid-structure equilibrium is given an initial small disturbance, the generated oscillations will either decay or diverge, depending on whether the flow energy transmitted to the structure is less than or surpass the energy dissipated by the damping of the system. If the fluid is at rest, any oscillation caused by the disturbance will be damped (for instance, by the fluid viscosity). When the velocity of the flow is augmented gradually the damping of the oscillations increases. However, with further increase in the flow velocity, a point is reached from where the system is no longer subject to damping. The oscillation just maintain its amplitude at the point where the damping vanishes. Above this point, any small disturbance generates oscillations of large amplitude. This is a flutter instability. Moreover, the point where the damping reduces to zero is referred to flutter boundary.

Flutter instabilities can take place in a great number of civil engineering processes: heat exchanger tubes in axial flow, flexible pipes with internal flow, wind effects on long span bridges, aircraft wings and so forth. Such flow-induced vibrations can damage the structure concerned. For example, it may happen that the fluid forces feed energy into the vibrating structure progressively increasing the amplitude of the motion until the structure collapses. The failure of the Tacoma's Narrow bridge was due to flutter, see [40]. The analysis of flutter instabilities is a major concern in the design of civil engineering systems involving a fluid-structure coupling. Hence, a great number of experimental [35, 40, 46, 47] and numerical [36, 33, 37] works have been carried out on this subject.

In this work we treat the flutter problem of a coupled fluid-structure system involving an incompressible Newtonian fluid and a reduced structure. This is carried out by a linear stability approach. We use the *Linearization Principle* formulation developed in Part I [16], particularly suited for fluid-structure problems involving moving boundaries. Thus, the analysis of the above flow-induced vibrations reduces to the computation of the leftmost eigenvalues of a coupled spectral problem, see [16, Section 3]. This coupled eigenproblem involves the linearized incompressible Navier-Stokes equations (written in a

fixed domain) and those of a reduced linear structure. The coupling is realized through specific transpiration interface conditions (see [14]).

We must notice that the use of a linear model for flutter analysis was already addressed (see for instance [33]). However, the originality of our approach lies in the linearization-transpiration formulation developed in Part I [16] which provides a coupled eigenproblem of minimal complexity, involving transpiration interface conditions. In this sense, the present paper constitutes the numerical counterpart of the mentioned formulation. The eigenproblem is discretized using a finite element approximation, and its smallest real part eigenvalues are approximated by combining a generalized Cayley transform and an Implicit Restarted Arnoldi Method. Finally, several numerical experiments will point out, on the one hand, the performance of our approximation scheme and, on the other hand, the robustness of our linearization-transpiration formulation for flutter instabilities detection.

The outline of this paper is as follows. In section 2 we introduce the spectral problem arising from the linearization-transpiration formulation developed in Part I [16]. In section 3 this problem is approximated using a stabilized finite element method. To this end a mixed variational formulation of the differential problem is introduced. The velocity and pressure are both approximated using continuous functions with $\mathbb{P}_1$ interpolation per element. The discrete formulation leads to a sparse generalized eigenvalues problem. In section 4 we deal with the leftmost eigenvalues computation of this generalized eigenproblem. We briefly discuss the IRAM method and the generalized Cayley transform. We summarize the main steps of the Cayley transform Arnoldi algorithm (introduced in [30]) and we provide some implementation techniques for the matrix-vector operations. Finally, the numerical experiments are reported in section 5. We consider three situations: a structure immersed in a fluid at rest, a cantilever pipe conveying a fluid flow and a rectangular bridge deck profile under wind effects. The numerical results are compared to former approaches and experimental data.

2 Linear stability: spectral problem

We consider a steady fluid-structure equilibrium. In this configuration, the solid is located in a domain $\Omega^{\rm s} \subset \mathbb{R}^3$ with boundary γ. As in many problems of aeroelasticity at low Mach numbers, it is surrounded by a fluid in $\mathbb{R}^3$. We introduce a control volume $\Omega \subset \mathbb{R}^3$ containing the solid. Hence, the fluid evolution is restricted to the domain $\Omega^{\rm f} = \Omega - \overline{\Omega}^{\rm s}$. In the sequel we set $\Gamma = \partial\Omega$ with $\Gamma = \Gamma_{\rm in} \cup \Gamma_{\rm out}$, $\Gamma_{\rm in} \cap \Gamma_{\rm out} = \emptyset$. Here, $\Gamma_{\rm in}$ stands for the inlet boundary and $\Gamma_{\rm out}$ for the outlet boundary, see figure 1.

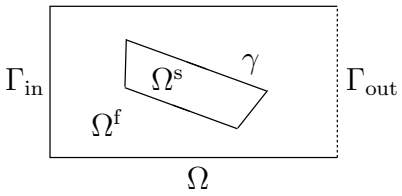

Figure 1: The computational domain Ω, defined by the system in its equilibrium configuration

We assume the fluid to be newtonian viscous, homogeneous and incompressible. Its behavior is described by its velocity u_0 and pressure p_0. At equilibrium, these fields satisfy the following incompressible Navier-Stokes equations written in eulerian conservative formulation in the unknown conifuration $\Omega = \Omega^{\rm f} \cup \overline{\Omega}^{\rm s}$:

$$\begin{aligned} \operatorname{div}\left(u_0 \otimes u_0 - \frac{1}{\rho}\sigma(u_0, p_0)\right) &= 0, \quad \text{in} \quad \Omega^{\rm f}, \\ \operatorname{div} u_0 &= 0, \quad \text{in} \quad \Omega^{\rm f}, \\ u_0 &= u_{\Gamma_{\rm in}}, \quad \text{on} \quad \Gamma_{\rm in}, \\ \sigma(u_0, p_0)n &= 0, \quad \text{on} \quad \Gamma_{\rm out}, \\ u_0 &= 0, \quad \text{on} \quad \gamma, \end{aligned} \tag{1}$$

with

$$\varepsilon(u_0) = \frac{1}{2}\left[\nabla u_0 + (\nabla u_0)^{\rm T}\right], \quad \sigma(u_0, p_0) = -p_0\,{\rm I} + 2\mu\varepsilon(u_0),$$

$\rho > 0$ stands for the volume fluid density, μ for the kinetic viscosity of the fluid, n for the unit normal vector on Γ pointing inside $\Omega^{\rm s}$, and $u_{\Gamma_{\rm in}}$ for the fixed velocity on $\Gamma_{\rm in}$. Since, at equilibrium the structure is at rest, the interface condition $(1)_5$ expresses the continuity of the velocity field at the fluid-structure interface. In the sequel we will suppose that u_0 and p_0 are smooth functions.

The elastic solid under large displacements is described by its velocity and its stress tensor. As in [16], in this paper we will suppose that the displacement of the structure, around a known configuration $\Omega^{\rm s}_0$, is given by a linear combination of a finite number of vibration modes $\varphi_i : \Omega^{\rm s}_0 \longrightarrow \mathbb{R}^3, \quad 1 \leq i \leq n^{\rm s}$, in such a way that the motion of the structure can be written as $I_{\Omega^{\rm s}_0} + \Phi s$ in $\Omega^{\rm s}_0$, with $s \in \mathbb{R}^{n^{\rm s}}$ and $\Phi = [\varphi_1 | \varphi_2 | \ldots | \varphi_{n^{\rm s}}]$ is a $3 \times n^{\rm s}$ matrix standing for the reduced modal basis. In this way, the structural behavior is driven by given mass and stiffness operators, $\mathcal{M}$ and $\mathcal{K}$ respectively. Thus, the equation describing the steady equilibrium of the structure subject to fluid effects is given by

$$\mathcal{K} s_0 = - \int_\gamma \Phi^{\rm T} \sigma(u_0, p_0) n \, {\rm d}a, \tag{2}$$

where s_0 stands for the generalized coordinates of the structural displacement. It equilibrates the fluid load at the interface γ.

Remark 2.1 *In the particular case where the configuration at the equilibrium Ω is known, problems* (1) *and* (2) *are uncoupled (see numerical experiments below). However, in general, the equilibrium configuration Ω depends on the structural displacement s_0, and then problems* (1) *and* (2) *are strongly coupled (see [9]).*

In this paper we focus on the numerical solution of the following quadratic eigenvalue problem: find the pulsation $\lambda \in \mathbb{C}$, the perturbation velocity $u : \Omega^{\rm f} \longrightarrow \mathbb{C}^3$, pressure $p : \Omega^{\rm f} \longrightarrow \mathbb{C}$ and displacement parametrization $s \in \mathbb{C}^{n^{\rm s}}$, with $(u, p, s) \neq 0$, such that

$$
\begin{aligned}
\nabla u_0 u + \nabla u u_0 - 2\nu \operatorname{div} \varepsilon(u) + \frac{1}{\rho}\nabla p = \lambda u, \quad & \text{in} \quad \Omega^{\mathrm{f}}, \\
\operatorname{div} u = 0, \quad & \text{in} \quad \Omega^{\mathrm{f}}, \\
u = 0, \quad & \text{on} \quad \Gamma_{\mathrm{in}}, \\
\sigma(u,p)n = 0, \quad & \text{on} \quad \Gamma_{\mathrm{out}}, \\
u = -\lambda \Phi s - \nabla u_0 \Phi s, \quad & \text{on} \quad \gamma, \\
\lambda^2 \,\mathrm{M}\, s + \left(\mathrm{K} + \mathrm{B}^0\right) s = -\int_\gamma \Phi^{\mathrm{T}} \sigma(u,p) n \,\mathrm{d}a, &
\end{aligned}
\tag{3}
$$

where M and K denote, respectively, the tangential mass and stiffness matrices of the structure and B^0 is a $n^{\mathrm{s}} \times n^{\mathrm{s}}$ real geometric matrix, given by the following expression:

$$
\mathrm{B}^0_{ij} = \int_\gamma \left\{ \nabla\sigma(u_0,p_0)\varphi_j n + \sigma(u_0,p_0)\left[\mathrm{I}\operatorname{div}\varphi_j - (\nabla\varphi_j)^{\mathrm{T}}\right] n \right\} \cdot \varphi_i \,\mathrm{d}a, \tag{4}
$$

for $1 \le i, j \le n^{\mathrm{s}}$.

Spectral problem (3) arises from the linear stability analysis of the fluid-structure equilibrium state (u_0, p_0, s_0), satisfying equations (1) and (2). This eigenproblem was derived in Part I [16, Section 3.3] (see also [15, Chapter 4]) by combining the "Linearization Principle" approach (see [22]) with the recent linearization method developed in [14, 15], particularly suited for problems involving moving boundaries. In this way, the above steady equilibrium state will be considered linearly asymptotically stable, if eigenproblem (3) does not have eigenvalues with negative real part. However, this steady state will be termed unstable if there exists, at least, one eigenvalue with negative real part.

Remark 2.2 *The transpiration boundary condition* $(3)_5$ *and the above "added stiffness" matrix* B^0 *come from the geometric interaction between the fluid and the structure, refer to [16, 14, 15], and take into account the possible motion of the interface.*

3 Numerical analysis

After the mathematical analysis reported in Part I [16, Section 4], we address, in this section, the finite element discretization of the eigenvalue problem (3). We first rewrite the "fluid part" of (3) in variational form and then we propose a stabilized finite element approximation. Finally, we provide the corresponding matrix formulation, which leads to a sparse generalized eigenvalue problem.

3.1 Variational formulation

In the sequel we consider functions defined in bounded subsets of $\mathbb{R}^3$, and taking values in the complex field $\mathbb{C}$. Thus, all L^p and Sobolev spaces appearing in this section are taken as complex vector spaces of functions with complex values, see [10]. Let Ω be an open bounded subset of $\mathbb{R}^3$, with locally Lipschitz continuous boundary $\Gamma = \Gamma_{\rm in} \cup \Gamma_{\rm out}$. We assume that $\Omega^{\rm s}$ is a non-empty connected open subset of Ω, with locally Lipschitz continuous boundary γ, and such that $\overline{\Omega^{\rm s}} \subset \Omega$, see figure 1.

Introducing the change of variables $z = -\lambda s$, eigenproblem (3) takes the following traditional form (see also Part I [16, Section 4.2.1]): find $\lambda \in \mathbb{C}$, $u : \Omega^{\rm f} \longrightarrow \mathbb{C}^3$, $p : \Omega^{\rm f} \longrightarrow \mathbb{C}$ and $s, z \in \mathbb{C}^{n^{\rm s}}$, with $(u, p, s, z) \neq 0$, such that

$$
\begin{aligned}
\rho\big(\nabla u_0 u + \nabla u u_0\big) - 2\mu \,\mathrm{div}\,\varepsilon(u) + \nabla p &= \lambda \rho u, \quad \text{in} \quad \Omega^{\rm f},\\
\mathrm{div}\, u &= 0, \quad \text{in} \quad \Omega^{\rm f},\\
u &= 0, \quad \text{on} \quad \Gamma_{\rm in},\\
\sigma(u,p)n &= 0, \quad \text{on} \quad \Gamma_{\rm out},\\
u = \Phi z - \nabla u_0 \Phi s, &\quad \text{on} \quad \gamma,\\
-z &= \lambda s,\\
\big(\mathrm{K} + \mathrm{B}^0\big)\, s + \int_\gamma \Phi^{\rm T} \sigma(u,p) n \,\mathrm{d}a &= \lambda\, \mathrm{M}\, z.
\end{aligned}
\tag{5}
$$

We consider the following complex Sobolev spaces:

$$
\begin{aligned}
H^1_{\Gamma_{\rm in}}(\Omega^{\rm f}) &= \big\{ v \in H^1(\Omega^{\rm f}) | v = 0, \quad \text{on} \quad \Gamma_{\rm in} \big\},\\
H^1_{\Gamma_{\rm in}\cup\gamma}(\Omega^{\rm f}) &= \big\{ v \in H^1(\Omega^{\rm f}) | v = 0, \quad \text{on} \quad \Gamma_{\rm in} \cup \gamma \big\},
\end{aligned}
$$

and a linear continuous lift operator

$$R : H^{\frac{1}{2}}(\gamma)^3 \longrightarrow H^1_{\Gamma_{\rm in}}(\Omega^{\rm f})^3. \tag{6}$$

By multiplying equation $(5)_1$ by $v \in H^1_{\Gamma_{\rm in}\cup\gamma}(\Omega^{\rm f})^3$, integrating by parts and taking into account the boundary conditions, we get that eigenvalue problem (5) can be written, under variational form, in the following way: find $\lambda \in \mathbb{C}$ and $(u, p, s, z) \neq 0$ in $H^1(\Omega^{\rm f})^3 \times L^2(\Omega^{\rm f}) \times \mathbb{C}^{n^{\rm s}} \times \mathbb{C}^{n^{\rm s}}$ such that

$$\begin{aligned} u - R(\Phi z - \nabla u_0 \Phi s) &\in H^1_{\Gamma_{\rm in}\cup\gamma}(\Omega^{\rm f})^3, \\ a(u,v) + b(p,v) &= \lambda d(u,v), \quad \forall v \in H^1_{\Gamma_{\rm in}\cup\gamma}(\Omega^{\rm f})^3, \\ b(q,u) &= 0, \quad \forall q \in L^2(\Omega^{\rm f}), \\ -z &= \lambda s, \\ \left(\mathrm{K} + \mathrm{B}^0\right) s + \int_\gamma \Phi^{\rm T} \sigma(u,p) n \,\mathrm{d}a &= \lambda \,\mathrm{M}\, z, \end{aligned} \tag{7}$$

with notation

$$\begin{aligned} a(u,v) &= \rho(\nabla u_0 u + \nabla u u_0, \bar{v})_{0,\Omega^{\rm f}} + 2\mu(\varepsilon(u), \varepsilon(\bar{v}))_{0,\Omega^{\rm f}}, \\ d(u,v) &= \rho(u, \bar{v})_{0,\Omega^{\rm f}}, \\ b(p,v) &= -(p, \operatorname{div} \bar{v})_{0,\Omega^{\rm f}}. \end{aligned}$$

Note that the surface integral in $(7)_5$,

$$\int_\gamma \Phi^{\rm T} \sigma(u,p) n \,\mathrm{d}a, \tag{8}$$

must be taken in the sens of $H^{-\frac{1}{2}}(\Gamma \cup \gamma)^{n^{\rm s}}$, i.e. the i-th component of (8) is defined as

$$\int_\gamma \big(\sigma(u,p)n\big) \cdot \varphi_i \,\mathrm{d}a = \langle \sigma(u,p)n, \chi_\gamma(\varphi_i) \rangle_{H^{-\frac{1}{2}}(\Gamma\cup\gamma), H^{\frac{1}{2}}(\Gamma\cup\gamma)},$$

for $i = 1, \ldots, n^{\rm s}$ and with

$$\chi_\gamma(\varphi) = \begin{cases} 0 & \text{on} \quad \Gamma \\ \varphi & \text{on} \quad \gamma \end{cases}.$$

This definition makes sense because, from $(7)_2$,

$$\operatorname{div}\sigma(u,p) \in L^2(\Omega^{\mathrm{f}}), \tag{9}$$

and then $\sigma(u,p)n \in H^{-\frac{1}{2}}(\Gamma \cup \gamma)$, see for instance [23]. In a discrete framework this condition does not generally hold. Therefore, we have to specify rigorously the discrete counterpart of (8). Basically, the idea consists in treating the surface integral as a variational residual, see [28]. Indeed, by multiplying $(5)_1$ by $R(\varphi_i)$, integrating by parts and taking into account the boundary conditions, we get

$$\int_\gamma \big(\sigma(u,p)n\big)\cdot\varphi_i \,\mathrm{d}a = a(u,R(\varphi_i)) + b(p,R(\varphi_i)) - \lambda d(u,R(\varphi_i)). \tag{10}$$

Clearly, the right hand side of (10) is better adapted to a finite element discretization than the left one. Taking into account (10), we can rewrite (7) in the following way: find $\lambda \in \mathbb{C}$ and $(u,p,s,z) \neq 0$ in $H^1(\Omega^{\mathrm{f}})^3 \times L^2(\Omega^{\mathrm{f}}) \times \mathbb{C}^{n^{\mathrm{s}}} \times \mathbb{C}^{n^{\mathrm{s}}}$ such that

$$\begin{aligned}
u - R(\Phi z - \nabla u_0 \Phi s) &\in H^1_{\Gamma_{\mathrm{in}}\cup\gamma}(\Omega^{\mathrm{f}})^3,\\
a(u,v) + b(p,v) &= \lambda d(u,v), \quad \forall v \in H^1_{\Gamma_{\mathrm{in}}\cup\gamma}(\Omega^{\mathrm{f}})^3,\\
b(q,u) &= 0, \quad \forall q \in L^2(\Omega^{\mathrm{f}}),\\
-z &= \lambda s,\\
\big(\mathrm{K}+\mathrm{B}^0\big)\, s + F^a(u) + F^b(p) &= \lambda\left(\mathrm{M}\, z + F^d(u)\right),
\end{aligned} \tag{11}$$

with $F^a(u), F^b(p), F^d(u) \in \mathbb{C}^{n^{\mathrm{s}}}$ given, from (10), by the following expressions:

$$\big[F^a(u)\big]_i = a(u,R(\varphi_i)), \quad \big[F^b(p)\big]_i = b(p,R(\varphi_i)), \quad \big[F^d(u)\big]_i = d(u,R(\varphi_i)),$$

far $i = 1,\ldots,n^{\mathrm{s}}$.

3.2 Finite element discretization

In the sequel, we will assume that $\Omega^{\mathrm{f}} \subset \mathbb{R}^3$ is a polygonal domain with which we associate a regular family of triangulations $\{\mathcal{T}_h\}_{h>0}$ (see [5]), such that

$$\overline{\Omega}^{\mathrm{f}} = \bigcup_{K\in\mathcal{T}_h} K, \quad \forall h > 0,$$

where h is defined by $h = \max_{K \in \mathcal{T}_h} h_k$, with h_k the diameter of K.

In order to approximate the continuous spaces $H^1(\Omega^{\rm f})$ and $L^2(\Omega^{\rm f})$, we introduce the finite dimensional space V_h defined by

$$V_h = \left\{ v_h \in \mathcal{C}^0(\overline{\Omega}^{\rm f}) |\, v_{h|K} \in \mathbb{P}_1(K), \quad \forall K \in \mathcal{T}_h \right\},$$

where $\mathbb{P}_1(K)$ stands for the space of polynomials on K of degree less or equal to 1. Thus, we define the following discrete spaces:

$$X_h = V_h \cap H^1_{\Gamma_{\rm in}}(\Omega^{\rm f}), \quad Q_h = V_h, \quad V_{h,0} = V_h \cap H^1_{\Gamma_{\rm in} \cup \gamma}(\Omega^{\rm f}). \tag{12}$$

In a discrete framework, the operator R in (6) is replaced by a discrete lift operator

$$R_h : {\rm Tr}(V_h)^3_{|\gamma} \longrightarrow X_h^3.$$

In the same way, we introduce a $\mathbb{P}_1$ Lagrange-piecewise interpolation operator P_h on γ

$$P_h : \mathcal{C}^0(\gamma)^3 \longrightarrow {\rm Tr}(V_h)^3_{|\gamma},$$

defined as the restriction on γ of the classical $\mathbb{P}_1$ Lagrange-piecewise interpolation operator Π_h in $\Omega^{\rm f}$.

With this notation, we can approximate problem (11), by replacing the continuous spaces $H^1(\Omega^{\rm f})^3$ and $L^2(\Omega^{\rm f})$ by the discrete spaces V_h and Q_h, (see [7]). Hence, we obtain the following approximate problem: find $\lambda \in \mathbb{C}$ and $(u, p, s, z) \neq 0$ in $V_h^3 \times Q_h \times \mathbb{C}^{n^{\rm s}} \times \mathbb{C}^{n^{\rm s}}$ such that

$$\begin{aligned}
u - R_h P_h(\Phi z - \nabla u_0 \Phi s) &\in V_{h,0}^3, \\
a(u, v) + b(p, v) &= \lambda d(u, v), \quad \forall v \in V_{h,0}^3, \\
b(q, u) &= 0, \quad \forall q \in Q_h, \\
-z &= \lambda s, \\
\left({\rm K} + {\rm B}^0 \right) s + F_h^a(u) + F_h^b(p) &= \lambda \left({\rm M}\, z + F_h^d(u) \right),
\end{aligned} \tag{13}$$

with $F_h^a(u), F_h^b(p), F_h^d(u) \in \mathbb{C}^{n^{\rm s}}$ given by

$$\begin{aligned}
\left[F_h^a(u) \right]_i &= a(u, R_h P_h(\varphi_i)), \\
\left[F_h^b(p) \right]_i &= b(p, R_h P_h(\varphi_i)), \\
\left[F_h^d(u) \right]_i &= d(u, R_h P_h(\varphi_i)),
\end{aligned}$$

for $i = 1, \ldots, n^{\mathrm{s}}$.

As we have already pointed out in Part I [16, paragraph 4.2.3], and as it will be confirmed below (in section 4.4), the solution of problem (13), involves a $\mathbb{P}_1/\mathbb{P}_1$ mixed finite element approximation of linearized Navier-Stokes problems with right hand side and zero order reaction term,

$$\begin{aligned} \rho\big(\nabla u_0 u + \nabla u u_0\big) - 2\mu \operatorname{div} \varepsilon(u) + \nabla p + r\rho u = \rho f, \quad & \text{in} \quad \Omega^{\mathrm{f}}, \\ \operatorname{div} u = 0, \quad & \text{in} \quad \Omega^{\mathrm{f}}, \\ u = 0, \quad & \text{on} \quad \Gamma_{\mathrm{in}}, \\ \sigma(u,p)n = 0, \quad & \text{on} \quad \Gamma_{\mathrm{out}}, \\ u = u_\gamma, \quad & \text{on} \quad \gamma, \end{aligned} \tag{14}$$

with $r \in \mathbb{R}$, f and u_γ given data.

The pair of spaces $\mathbb{P}_1/\mathbb{P}_1$, chosen to discretize the velocity and pressure fields, fail to satisfy the LBB compatibility condition (Ladyzhenskaya-Babuska-Brezzi or "inf-sup" condition), see [23]. It is well known that, if this condition does not hold, the numerical scheme produces oscillating pressures (see for instance [12]). The "stabilized finite element methods" overcome this problem. The goal is to enhance stability (introducing diffusion) without upsetting the consistency (see [26]).

We could use a combination of spaces satisfying the LBB condition, but the numerical approximation of convection-diffusion (or Navier-Stokes) equations, with low-order piecewise polynomials, may also produce severely oscillating solutions. A number of stabilization techniques have been developed for the treatment of this problem, see for instance [2, 25, 45]. Similar difficulties may appear when dealing with dominating reaction terms. Again, some techniques of stabilization have been developed for this purpose, but for particular cases where the reaction reduces to a scalar constant [43, 17, 24, 1].

The stabilized schemes are generally obtained, from the classical Galerkin method (not-stabilized), by adding additional terms involving the product of the residual of the equation with a new test function which depends on a local stabilization parameter, $\tau_K > 0$. Unfortunately, to our present knowledge, there is no a stabilized finite element method for the discretization of a general problem of type (14), see [44]. The discretization scheme that we propose herein for (14) is directly obtained from that proposed in [45] for the Oseen's

equations and writes: find $(u,p) \in V_h^3 \times Q_h$ such that

$$
\begin{aligned}
& u - R_h P_h(u_\gamma) \in V_{h,0}^3, \\
& a(u,v) + b(p,v) + b(q,u) + r\rho(u,v)_{0,\Omega} \\
& \quad + \sum_{K \in \mathcal{T}_h} \Big(\rho(\nabla u_0 u + \nabla u u_0) - 2\mu \operatorname{div} \varepsilon(u) + \nabla p + r\rho u, \\
& \qquad \tau_K(\rho \nabla v u_0 - 2\mu \operatorname{div} \varepsilon(v) - \nabla q) \Big)_{0,K} \\
& = d(f,v) + \sum_{K \in \mathcal{T}_h} \Big(\rho f, \tau_K(\rho \nabla v u_0 - 2\mu \operatorname{div} \varepsilon(v) - \nabla q) \Big)_{0,K}, \\
& \quad \forall (v,q) \in V_{h,0}^3 \times Q_h,
\end{aligned}
\tag{15}
$$

with τ_K the stabilization parameter provided in [45],

$$
\tau_K = \frac{h_K}{2\rho \|u_0\|_2} \xi(\mathcal{R}_h e_K), \quad \mathcal{R}_h e_K = \frac{\|u_0\|_2 h_K}{12\nu}, \quad \xi(x) = \begin{cases} x & \text{si} \quad 0 \le x < 1 \\ 1 & \text{si} \quad x \ge 1 \end{cases} .
$$

Several reasons justify the introduction of the above scheme. On the one hand, we have employed the same triangulation $\mathcal{T}_h$ in the computation of u_0 and u (it is not mandatory, but practical). Thus, an accurate computation of the permanent flow (u_0, p_0) and of $(\nabla u_0)_{|\gamma}$, requires a refined grid in the vicinity of γ. As pointed out in [17], this reduces the complications associated when dealing with dominating reaction terms. Moreover, scheme (15) is a direct extension of those introduced in [43] and [45] for the Stokes equations with convection. In this way, we have kept the choice of τ_K for this type of equations as proposed in [45]. On the oder hand, the numerical experiments reported in section 5 will point out the performance of scheme (15).

Remark 3.1 *It is straigtforward to verify that* (15) *is consistent with the solutions of* (14).

By generalizing (15), we consider instead of (13) the following discrete scheme: find $\lambda \in \mathbb{C}$ and $(u,p,s,z) \neq 0$ in $V_h^3 \times Q_h \times \mathbb{C}^{n^s} \times \mathbb{C}^{n^s}$ such that

$$
\begin{aligned}
&u - R_h P_h(\Phi z - \nabla u_0 \Phi s) \in V_{h,0}^3,\\
&a(u,v) + b(p,v) + \overline{b(q,u)}\\
&\qquad + \sum_{K\in\mathcal{T}_h} \Big(\rho(\nabla u_0 u + \nabla u u_0) + \nabla p, \tau_K(\rho\nabla\bar{v}u_0 - \nabla\bar{q})\Big)_{0,K}\\
&\quad = \lambda\left[d(u,v) + \sum_{K\in\mathcal{T}_h}\Big(\rho u, \tau_K(\rho\nabla\bar{v}u_0 - \nabla\bar{q})\Big)_{0,K}\right], \quad \forall (v,q)\in V_{h,0}^3\times Q_h,\\
&-z = \lambda s,\\
&\left(\mathrm{K}+\mathrm{B}^0\right)s + F_h^a(u) + F_h^b(p) = \lambda\left(\mathrm{M}\,z + F_h^d(u)\right),
\end{aligned}
\tag{16}
$$

with

$$
\begin{aligned}
\left[F_h^a(u)\right]_i &= a(u, R_hP_h(\varphi_i)) + \sum_{K\in\mathcal{T}_h}\Big(\rho(\nabla u_0 u + \nabla u u_0), \tau_K\rho\nabla(R_hP_h(\varphi_i))u_0\Big)_{0,K},\\
\left[F_h^b(p)\right]_i &= b(p, R_hP_h(\varphi_i)) + \sum_{K\in\mathcal{T}_h}\Big(\nabla p, \tau_K\rho\nabla(R_hP_h(\varphi_i))u_0\Big)_{0,K},\\
\left[F_h^d(u)\right]_i &= d(u, R_hP_h(\varphi_i)) + \sum_{K\in\mathcal{T}_h}\Big(\rho u, \tau_K\rho\nabla(R_hP_h(\varphi_i))u_0\Big)_{0,K},
\end{aligned}
$$

for $i = 1, \ldots, n^{\mathrm{s}}$.

Remark 3.2 *For each $u \in V_h^3$ we have $u_{|K} \in \mathbb{P}_1^3(K)$ and then* $\operatorname{div}\varepsilon(u)$ *vanishes in K*

By setting

$$
\begin{aligned}
a_s(u,v) &= \sum_{K\in\mathcal{T}_h}\Big(\rho(\nabla u_0 u + \nabla u u_0), \tau_K\rho\nabla\bar{v}u_0\Big)_{0,K},\\
b_s(p,v) &= \sum_{K\in\mathcal{T}_h}\Big(\nabla p, \tau_K\rho\nabla\bar{v}u_0\Big)_{0,K},\\
b_s^t(u,q) &= -\sum_{K\in\mathcal{T}_h}\Big(\rho(\nabla u_0 u + \nabla u u_0), \tau_K\nabla\bar{q}\Big)_{0,K},
\end{aligned}
$$

$$
\begin{aligned}
c_s(p,q) &= -\sum_{K\in\mathcal{T}_h}\Big(\nabla p, \tau_K\nabla\bar{q}\Big)_{0,K},\\
d_s(u,v) &= \sum_{K\in\mathcal{T}_h}\Big(\rho u, \tau_K\rho\nabla\bar{v}u_0\Big)_{0,K},\\
e_s(u,q) &= -\sum_{K\in\mathcal{T}_h}\Big(\rho u, \tau_K\nabla\bar{q}\Big)_{0,K},
\end{aligned}
$$

problem (16) can be written in the following more compact form: find $\lambda\in\mathbb{C}$ and $(u,p,s,z)\neq 0$ in $V_h^3\times Q_h\times\mathbb{C}^{n^{\rm s}}\times\mathbb{C}^{n^{\rm s}}$ such that

$$
\begin{aligned}
&u - R_h(\Phi z - \nabla u_0\Phi s)\in V_{h,0}^3,\\
&a(u,v)+b(p,v)+\overline{b(q,u)}+a_s(u,v)+b_s(p,v)+b_s^t(q,u)+c_s(p,q)\\
&\quad=\lambda\big(d(u,v)+d_s(u,v)+e_s(q,u)\big),\quad \forall (v,q)\in V_{h,0}^3\times Q_h,\\
&-z=\lambda s,\\
&\big(\mathrm{K}+\mathrm{B}^0\big)\,s+F_h^a(u)+F_h^b(p)=\lambda\left(\mathrm{M}\,z+F_h^d(u)\right).
\end{aligned}
\tag{17}
$$

3.3 Matrix formulation

In this paragraph, problem (17) is reformulated in terms of matrices. This will allow us to explicitly compute its solutions. Let $n^{\rm f}=n^{\rm f}(h)$ the number of vertex of the triangulation $\mathcal{T}_h$ on the fluid domain. We introduce the finite element real basis $\{\phi_i\}_{i=1}^{3n^{\rm f}}$ and $\{\psi_i\}_{i=1}^{n^{\rm f}}$ of V_h^3 and Q_h respectively. Thus, each element $(u,p)\in V_h^3\times Q_h$ can be written as

$$
u=\sum_{j=1}^{3n^{\rm f}}u_j\phi_j,\quad p=\sum_{j=1}^{n^{\rm f}}p_j\psi_j,
\tag{18}
$$

with $u_j,p_j\in\mathbb{C}$. We introduce also the following subsets of $I=\{1,\dots,3n^{\rm f}\}\subset\mathbb{N}$:

$$
\begin{aligned}
I^{\Omega^{\rm f}}&=\{i\in I|\,\text{d.o.f. } i \text{ is not on } \Gamma\cup\gamma\},\quad I^{\Gamma_{\rm out}}=\{i\in I|\,\text{d.o.f. } i \text{ is on } \Gamma_{\rm out}\},\\
I^{\Gamma_{\rm in}}&=\{i\in I|\,\text{d.o.f. } i \text{ is on } \Gamma_{\rm in}\},\qquad\qquad I^{\gamma}=\{i\in I|\,\text{d.o.f. } i \text{ is on } \gamma\},
\end{aligned}
$$

and then we denote

$$n^{\Omega^{\rm f}} = \mathrm{card}(I^{\Omega^{\rm f}}), \quad n^{\Gamma_{\rm out}} = \mathrm{card}(I^{\Gamma_{\rm out}}), \quad n^{\Gamma_{\rm in}} = \mathrm{card}(I^{\Gamma_{\rm in}}), \quad n^{\gamma} = \mathrm{card}(I^{\gamma}).$$

By substituting (18) in $(17)_2$ we get

$$\begin{aligned}\sum_{j=1}^{3n^{\rm f}} u_j a(\phi_j, v) + \sum_{j=1}^{n^{\rm f}} p_j b(\psi_j, v) + \sum_{j=1}^{3n^{\rm f}} u_j \overline{b(q, \phi_j)} + \sum_{j=1}^{3n^{\rm f}} u_j a_s(\phi_j, v) \\ + \sum_{j=1}^{n^{\rm f}} p_j b_s(\psi_j, v) + \sum_{j=1}^{3n^{\rm f}} u_j b_s^t(\phi_j, q) + \sum_{j=1}^{n^{\rm f}} p_j c_s(\psi_j, q) \\ = \lambda \left(\sum_{j=1}^{3n^{\rm f}} u_j d(\phi_j, v) + \sum_{j=1}^{3n^{\rm f}} u_j d_s(\phi_j, v) + \sum_{j=1}^{3n^{\rm f}} u_j e_s(\phi_j, q) \right), \\ \forall (v, q) \in V_{h,0}^3 \times Q_h. \quad (19)\end{aligned}$$

We denote by $u^{\Omega^{\rm f}} \in \mathbb{C}^{n^{\Omega^{\rm f}}}$, $u^{\Gamma_{\rm out}} \in \mathbb{C}^{n^{\Gamma_{\rm out}}}$, $u^{\Gamma_{\rm in}} \in \mathbb{C}^{n^{\Gamma_{\rm in}}}$ et $u^{\gamma} \in \mathbb{C}^{n^{\gamma}}$ the degrees of freedom of u corresponding, respectively, to shape functions in $I^{\Omega^{\rm f}}$, $I^{\Gamma_{\rm out}}$, $I^{\Gamma_{\rm in}}$ and I^{γ}. In the sequel we will assume that the shape functions $\{\phi_i\}_{i=1}^{3n^{\rm f}}$ are ordered in such a way that the first degrees of freedom correspond to $u^{\Omega^{\rm f}}$, next to $u^{\Gamma_{\rm out}}$, next to $u^{\Gamma_{\rm in}}$ and finally to u^{γ}.

By taking in (19) $v = \phi_i$, with $i \in I^{\Omega^{\rm f}} \cup I^{\Gamma_{\rm out}}$, and $q = \psi_i$, with $i = 1, \ldots, n^{\rm f}$, we obtain a $(n^{\Omega^{\rm f}} + n^{\Gamma_{\rm out}} + n^{\rm f}) \times (4n^{\rm f} + 2n^{\rm s})$ matrix expression of type

$$\begin{bmatrix} \mathrm{A}_1^{\Omega^{\rm f}} & \mathrm{A}_1^{\Gamma_{\rm out}} & \mathrm{A}_1^{\Gamma_{\rm in}} & \mathrm{A}_1^{\gamma} & \mathrm{B}_1 & 0 & 0 \\ \mathrm{A}_2^{\Omega^{\rm f}} & \mathrm{A}_2^{\Gamma_{\rm out}} & \mathrm{A}_2^{\Gamma_{\rm in}} & \mathrm{A}_2^{\gamma} & \mathrm{B}_2 & 0 & 0 \\ \mathrm{B}^{\Omega^{\rm f}} & \mathrm{B}^{\Gamma_{\rm out}} & \mathrm{B}^{\Gamma_{\rm in}} & \mathrm{B}^{\gamma} & \mathrm{C} & 0 & 0 \end{bmatrix} \begin{bmatrix} u^{\Omega^{\rm f}} \\ u^{\Gamma_{\rm out}} \\ u^{\Gamma_{\rm in}} \\ u^{\gamma} \\ p \\ z \\ s \end{bmatrix}$$

$$= \lambda \begin{bmatrix} \mathrm{D}_1^{\Omega^{\rm f}} & \mathrm{D}_1^{\Gamma_{\rm out}} & \mathrm{D}_1^{\Gamma_{\rm in}} & \mathrm{D}_1^{\gamma} & 0 & 0 & 0 \\ \mathrm{D}_2^{\Omega^{\rm f}} & \mathrm{D}_2^{\Gamma_{\rm out}} & \mathrm{D}_2^{\Gamma_{\rm in}} & \mathrm{D}_2^{\gamma} & 0 & 0 & 0 \\ \mathrm{E}^{\Omega^{\rm f}} & \mathrm{E}^{\Gamma_{\rm out}} & \mathrm{E}^{\Gamma_{\rm in}} & \mathrm{E}^{\gamma} & 0 & 0 & 0 \end{bmatrix} \begin{bmatrix} u^{\Omega^{\rm f}} \\ u^{\Gamma_{\rm out}} \\ u^{\Gamma_{\rm in}} \\ u^{\gamma} \\ p \\ z \\ s \end{bmatrix}. \quad (20)$$

In the same way, by substituting (18) in $(17)_4$ we get

$$\left(\mathrm{K}+\mathrm{B}^0\right) s + \sum_{j=1}^{3n^{\mathrm{f}}} u_j F_h^a(\phi_j) + \sum_{j=1}^{n^{\mathrm{f}}} p_j F_h^b(\psi_j) = \lambda \left(\mathrm{M}\, z + \sum_{j=1}^{3n^{\mathrm{f}}} u_j F_h^d(\phi_j) \right),$$

which leads to the following matrix expression of size $n^{\mathrm{s}} \times (4n^{\mathrm{f}} + 2n^{\mathrm{s}})$:

$$\begin{aligned} \left[\mathrm{F}_a^{\Omega^{\mathrm{f}}} \quad \mathrm{F}_a^{\Gamma_{\mathrm{out}}} \quad \mathrm{F}_a^{\Gamma_{\mathrm{in}}} \quad \mathrm{F}_a^{\gamma} \quad \mathrm{F}_b \quad 0 \quad \mathrm{K}+\mathrm{B}^0\right] & \begin{bmatrix} u^{\Omega^{\mathrm{f}}} \\ u^{\Gamma_{\mathrm{out}}} \\ u^{\Gamma_{\mathrm{in}}} \\ u^{\gamma} \\ p \\ z \\ s \end{bmatrix} \\ = \lambda \left[\mathrm{F}_d^{\Omega^{\mathrm{f}}} \quad \mathrm{F}_d^{\Gamma_{\mathrm{out}}} \quad \mathrm{F}_d^{\Gamma_{\mathrm{in}}} \quad \mathrm{F}_d^{\gamma} \quad 0 \quad \mathrm{M} \quad 0\right] & \begin{bmatrix} u^{\Omega^{\mathrm{f}}} \\ u^{\Gamma_{\mathrm{out}}} \\ u^{\Gamma_{\mathrm{in}}} \\ u^{\gamma} \\ p \\ z \\ s \end{bmatrix}. \end{aligned} \tag{21}$$

The transpiration interface condition $(17)_1$ is taken explicitly on each interface vertex, x_i, of the triangulation. Therefore, we obtain the following matrix expression of size $(n^{\Gamma_{\mathrm{in}}} + n^{\gamma}) \times (4n^{\mathrm{f}} + 2n^{\mathrm{s}})$:

$$\begin{bmatrix} 0 & 0 & \mathrm{I} & 0 & 0 & 0 & 0 \\ 0 & 0 & 0 & \mathrm{I} & 0 & -\mathrm{G}^0 & \mathrm{G}^1 \end{bmatrix} \begin{bmatrix} u^{\Omega^{\mathrm{f}}} \\ u^{\Gamma_{\mathrm{out}}} \\ u^{\Gamma_{\mathrm{in}}} \\ u^{\gamma} \\ p \\ z \\ s \end{bmatrix} = \lambda \begin{bmatrix} 0 & 0 & 0 & 0 & 0 & 0 & 0 \\ 0 & 0 & 0 & 0 & 0 & 0 & 0 \end{bmatrix} \begin{bmatrix} u^{\Omega^{\mathrm{f}}} \\ u^{\Gamma_{\mathrm{out}}} \\ u^{\Gamma_{\mathrm{in}}} \\ u^{\gamma} \\ p \\ z \\ s \end{bmatrix}, \tag{22}$$

with the following notation:

$$\begin{aligned} \left[\mathrm{G}^0\right]_{ij} &= [\varphi_j]_{\mathrm{nc}(i)}\,(x_{\mathrm{nv}(i)}), \qquad i \in I^{\Gamma_{\mathrm{in}}} \quad j = 1, \ldots, n^{\mathrm{s}}, \\ \left[\mathrm{G}^1\right]_{ij} &= [\nabla u_0 \varphi_j]_{\mathrm{nc}(i)}\,(x_{\mathrm{nv}(i)}), \qquad i \in I^{\gamma} \quad j = 1, \ldots, n^{\mathrm{s}}. \end{aligned}$$

Here, $\mathrm{nc}(i) \in \{1,2,3\}$ is the component of the velocity corresponding to the velocity degree of freedom i, and $\mathrm{nv}(i) \in \{1,\ldots,n^{\mathrm{f}}\}$ the label of the vertex where the velocity degree of freedom i lies, for $i = 1,\ldots,3n^{\mathrm{f}}$.

In short, taking into account $(17)_3$ with (20), (21) and (22) we obtain that the discrete problem (17) is equivalent to the following generalized eigenvalue problem of size $n = 4n^{\mathrm{f}} + 2n^{\mathrm{s}}$: find $\lambda \in \mathbb{C}$ and $0 \neq \mathrm{x} \in \mathbb{C}^n$ such that

$$\underbrace{\begin{bmatrix} \mathrm{A}_1^{\Omega^{\mathrm{f}}} & \mathrm{A}_1^{\Gamma_{\mathrm{out}}} & \mathrm{A}_1^{\Gamma_{\mathrm{in}}} & \mathrm{A}_1^{\gamma} & \mathrm{B}_1 & 0 & 0 \\ \mathrm{A}_2^{\Omega^{\mathrm{f}}} & \mathrm{A}_2^{\Gamma_{\mathrm{out}}} & \mathrm{A}_2^{\Gamma_{\mathrm{in}}} & \mathrm{A}_2^{\gamma} & \mathrm{B}_2 & 0 & 0 \\ 0 & 0 & \mathrm{I} & 0 & 0 & 0 & 0 \\ 0 & 0 & 0 & \mathrm{I} & 0 & -\mathrm{G}^0 & \mathrm{G}^1 \\ \mathrm{B}^{\Omega^{\mathrm{f}}} & \mathrm{B}^{\Gamma_{\mathrm{out}}} & \mathrm{B}^{\Gamma_{\mathrm{in}}} & \mathrm{B}^{\gamma} & \mathrm{C} & 0 & 0 \\ 0 & 0 & 0 & 0 & 0 & -\mathrm{I} & 0 \\ \mathrm{F}_a^{\Omega^{\mathrm{f}}} & \mathrm{F}_a^{\Gamma_{\mathrm{out}}} & \mathrm{F}_a^{\Gamma_{\mathrm{in}}} & \mathrm{F}_a^{\gamma} & \mathrm{F}_b & 0 & \mathrm{K}+\mathrm{B}^0 \end{bmatrix}}_{\mathrm{A}} \underbrace{\begin{bmatrix} u^{\Omega^{\mathrm{f}}} \\ u^{\Gamma_{\mathrm{out}}} \\ u^{\Gamma_{\mathrm{in}}} \\ u^{\gamma} \\ p \\ z \\ s \end{bmatrix}}_{\mathrm{x}}$$

$$= \lambda \underbrace{\begin{bmatrix} \mathrm{D}_1^{\Omega^{\mathrm{f}}} & \mathrm{D}_1^{\Gamma_{\mathrm{out}}} & \mathrm{D}_1^{\Gamma_{\mathrm{in}}} & \mathrm{D}_1^{\gamma} & 0 & 0 & 0 \\ \mathrm{D}_2^{\Omega^{\mathrm{f}}} & \mathrm{D}_2^{\Gamma_{\mathrm{out}}} & \mathrm{D}_2^{\Gamma_{\mathrm{in}}} & \mathrm{D}_2^{\gamma} & 0 & 0 & 0 \\ 0 & 0 & 0 & 0 & 0 & 0 & 0 \\ 0 & 0 & 0 & 0 & 0 & 0 & 0 \\ \mathrm{E}^{\Omega^{\mathrm{f}}} & \mathrm{E}^{\Gamma_{\mathrm{out}}} & \mathrm{E}^{\Gamma_{\mathrm{in}}} & \mathrm{E}^{\gamma} & 0 & 0 & 0 \\ 0 & 0 & 0 & 0 & 0 & 0 & \mathrm{I} \\ \mathrm{F}_d^{\Omega^{\mathrm{f}}} & \mathrm{F}_d^{\Gamma_{\mathrm{out}}} & \mathrm{F}_d^{\Gamma_{\mathrm{in}}} & \mathrm{F}_d^{\gamma} & 0 & \mathrm{M} & 0 \end{bmatrix}}_{\mathrm{B}} \underbrace{\begin{bmatrix} u^{\Omega^{\mathrm{f}}} \\ u^{\Gamma_{\mathrm{out}}} \\ u^{\Gamma_{\mathrm{in}}} \\ u^{\gamma} \\ p \\ z \\ s \end{bmatrix}}_{\mathrm{x}} \tag{23}$$

The matrices A and B are real, sparse, non-symmetric and, in most of the applications, of large size. Following the "Linearization Principle" approach developed in Part I [16, section 3], in a linear stability analysis the goal is to find eigenvalues with negative real part in order to detect instabilities. Typically, almost all eigenvalues of (23) have positive real part and only a small number cross the imaginary axis. Therefore, to detect a stability change, the interest lies in computing the few eigenvalues with smallest real part.

In the next section, we will deal with the numerical approximation of a small number (compared to n) of solutions of the generalized eigenproblem (23). To fully exploit the sparse character of the matrices, it will be crucial to use methods which only involve operations of type matrix-vector product (i.e.

which do not destroy the sparsity). For instance, subspace iteration methods or Arnoldi methods [3, 39] are very appropriate.

4 Eigenvalues computation

In this section we will follow the ideas of Garrat [19] and Lehoucq and Scott [30]. In this sense, the leftmost eigenvalues of (23) will be approximated using an iterative algorithm combining a generalized Cayley transform and an Implicit Restarted Arnoldi Method (IRAM). This algorithm is fully developed in [30]. This choice is justified, on the one hand, by the proven performance of the IRAM method, implemented in the ARPACK library [32], and on the other hand, by the results of Lehoucq and Scott [30] which point out the efficiency of their algorithm.

In the following paragraphs we will briefly describe the IRAM method and the generalized Cayely transform. We will summarize the main steps of the Cayley transform Arnoldi algorithm [30] provided with some implementation techniques used in the numerical experiments reported in section 5.

4.1 Generalized Cayley transform

A complication in problem (23) is the singularity of matrix B. This implies that (23) has fewer than n eigenvalues [19, 6]. The missing eigenvalues, called "infinite" eigenvalues [19, 42], are defined as the zero eigenvalues of the inverse problem

$$\mathrm{B}\,\mathrm{x} = \omega\,\mathrm{A}\,\mathrm{x}, \quad \omega = \frac{1}{\lambda}.$$

Each zero value of ω corresponds to an infinite eigenvalue of (23).

Since matrix B of (23) has one block of columns and two blocks of rows filled with zeros, eigenproblem (23) has three kinds of infinite eigenvalues. The pure pressures correspond to n^{f} columns of zeros. The two other groups of infinite eigenvalues, $n^{\Gamma_{\mathrm{in}}} + n^{\gamma}$, come from the explicit discrete treatment of the boundary conditions on Γ_{in} and γ, which are not implicitly incorporated in the discrete space V_h^3.

Although the infinite eigenvalues are not true eigenvalues of (23), in practice, they can introduce numerical difficulties [19, 6, 34, 30]. When working in

finite arithmetic, the matrix B is often perturbed so that it may become "not-singular". Eigenvalues with a very large module (and perhaps with negative real part) may appear which are, of course, irrelevant for the stability analysis.

Iterative methods for non symmetric problems, such as subspace iteration and Arnoldi, cannot be applied directly to the generalized eigenproblem (23). Before we must transform problem (23) in a standard problem of the form

$$\mathrm{T}\,\mathrm{x} = \theta\,\mathrm{x}\,. \tag{24}$$

The difficulty now is: to chose T. It is well known that iterative methods quickly provide good approximations to well-separated eigenvalues. In general, these eigenvalues do not match with those of smallest real part. ThusT must satisfy some *a priori* properties:

- matrix-vector products, $\mathrm{T}\,\mathrm{y}$, should be carried out efficiently;
- there is a known transformation between the solutions of (23) and (24);
- the eigenvalues with smallest real part of (23) are mapped to the eigenvalues of (24) which are easily approximated by the iterative method performed on (24).

The complication associated to the singularity of the matrix B also restricts the choice of the transformation T. We must use rational transformations, namely, it is necessary to invert problem (23). In this framework, standard choice when computing leftmost eigenvalues of problems like (23) are shift-invert and generalized Cayley transformation, see [12, 13, 30, 29].

In the sequel we will assume that (23) has m eigenvalues $\{\lambda_i\}_{i=1}^m$, which we suppose ordered with increasing order of their real parts,

$$\mathrm{Re}(\lambda_1) \leq \mathrm{Re}(\lambda_2) \leq \ldots \leq \mathrm{Re}(\lambda_m).$$

Let $\alpha \in \mathbb{C}$, with $\alpha \neq \lambda_i$ for $i = 1, \ldots, m$. By subtracting $\alpha\,\mathrm{B}\,\mathrm{x}$ from both sides of (23) we get

$$(\mathrm{A} - \alpha\,\mathrm{B})\,\mathrm{x} = (\lambda - \alpha)\,\mathrm{B}\,\mathrm{x}\,.$$

By multiplying this identity by $(\mathrm{A} - \alpha\,\mathrm{B})^{-1}$, we obtain

$$\underbrace{(\mathrm{A} - \alpha\,\mathrm{B})^{-1}\,\mathrm{B}}_{\mathrm{T}_{SI}(\alpha)}\,\mathrm{x} = \underbrace{\left(\frac{1}{\lambda - \alpha}\right)}_{\theta}\,\mathrm{x}\,. \tag{25}$$

The matrix $\mathrm{T}_{SI}(\alpha) = (\mathrm{A} - \alpha\,\mathrm{B})^{-1}\,\mathrm{B}$, is called shift-invert transformation. The eigenvectors of (23) and $\mathrm{T}_{SI}(\alpha)$ are identical. Hence, the eigenvalues λ of (23) and θ of $\mathrm{T}_{SI}(\alpha)$, are related by the following expression:

$$\lambda = \alpha + \frac{1}{\theta}, \quad \theta = \frac{1}{\lambda - \alpha}. \tag{26}$$

By selecting the shift (or pole) α near the imaginary axis, the left-most eigenvalues of (23) can be mapped onto those of $\mathrm{T}_{SI}(\alpha)$ with largest magnitude. However, since A and B are real matrices, and in order to keep the computation in real arithmetic, we will not consider the use of complex shifts, but generalized the shift-invert transformation.

Let $\alpha_1, \alpha_2 \in \mathbb{R}$ be such that

$$\alpha_1 < \alpha_2, \quad \alpha_1 \neq \lambda_i, \quad i = 1, \ldots, m. \tag{27}$$

By subtracting $\alpha_2\,\mathrm{B}\,\mathrm{x}$ from both sides of (23) we obtain

$$(\mathrm{A} - \alpha_2\,\mathrm{B})\,\mathrm{x} = (\lambda - \alpha_2)\,\mathrm{B}\,\mathrm{x}\,.$$

Let us suppose that x is an eigenvector and λ an eigenvalue of (23). By multiplying by $(\mathrm{A} - \alpha_1\,\mathrm{B})^{-1}$ we get

$$\underbrace{(\mathrm{A} - \alpha_1\,\mathrm{B})^{-1}(\mathrm{A} - \alpha_2\,\mathrm{B})}_{\mathrm{T}_C(\alpha_1,\alpha_2)}\mathrm{x} = (\lambda - \alpha_2)\,\underbrace{(\mathrm{A} - \alpha_1\,\mathrm{B})^{-1}\,\mathrm{B}}_{\mathrm{T}_{SI}(\alpha_1)}\mathrm{x} = \underbrace{\left(\frac{\lambda - \alpha_2}{\lambda - \alpha_1}\right)}_{\theta = c(\lambda)}\mathrm{x}\,. \tag{28}$$

The matrix

$$\mathrm{T}_C(\alpha_1, \alpha_2) = (\mathrm{A} - \alpha_1\,\mathrm{B})^{-1}(\mathrm{A} - \alpha_2\,\mathrm{B}), \tag{29}$$

is termed generalized Cayley transform, see [19, 20]. The scalars α_1 and α_2 are, respectively, referred to as pole and zero of the transformation. Transformation (29) is a generalization of the standard Cayley transform where $\alpha_1 = -\alpha_2$, see [18, 4].

From (28) we can easily derive the following lemma, giving the relationship between the finite eigenvalues of (23) and those of $\mathrm{T}_C(\alpha_1, \alpha_2)$, see [19].

Lemma 4.1 *Let $\alpha_1, \alpha_2 \in \mathbb{R}$ satisfying* (27). *The pair (λ, x) is an eigensolution of* (23) *if and only if (θ, x) is an eigensolution of $\mathrm{T}_C(\alpha_1, \alpha_2)$, where*

$$\theta = c(\lambda) = \frac{\lambda - \alpha_2}{\lambda - \alpha_1}, \quad \lambda = c^{-1}(\theta) = \frac{\alpha_1 \theta - \alpha_2}{\theta - 1}. \tag{30}$$

Here, c is a bijection of $\mathbb{C} - \{\alpha_1\}$ in $\mathbb{C} - \{1\}$.

The main interest of the generalized Cayley transform lies in the properties of the bijection c and the role of parameters α_1 and α_2 in this mapping. In particular, how do they affect the way the eigenvalues of (23) are mapped to those of $T_C(\alpha_1, \alpha_2)$. Garrat, in [19], provides a complete study of this mapping (see also [21]).

The main properties of the generalized Cayley transform can be summarized in the following theorem:

Theorem 4.2 (Garrat, 1991) *Let $\alpha_1, \alpha_2 \in \mathbb{R}$ with $\alpha_1 < \alpha_2$, and $\theta = c(\lambda)$ with $\lambda \in \mathbb{C} - \{\alpha_1\}$. Then*

$$\begin{aligned} \mathrm{Re}(\lambda) < \frac{1}{2}(\alpha_1 + \alpha_2) \quad &\textit{if and only if} \quad |\theta| > 1, \\ \mathrm{Re}(\lambda) \geq \frac{1}{2}(\alpha_1 + \alpha_2) \quad &\textit{if and only if} \quad |\theta| \leq 1. \end{aligned}$$

The above result implies that the eigenvalues of (23) lying on the left of the straight line $\mathrm{Re}(\lambda) = (\alpha_1 + \alpha_2)/2$ in the complex plan, are mapped to extreme eigenvalues of $\mathrm{T}_C(\alpha_1, \alpha_2)$.

More precisely, we have the following corollary (see [19]):

Corollary 4.3 *Let $\lambda_1, \lambda_2, \ldots, \lambda_m$ to be the eigenvalues of* (23) *ordered with increasing real parts. Take an index $1 \leq k < m$ such that $\mathrm{Re}(\lambda_k) < \mathrm{Re}(\lambda_{k+1})$. Let $\alpha_1, \alpha_2 \in \mathbb{R}$ satisfying* (27) *with*

$$\frac{1}{2}(\alpha_1 + \alpha_2) = \mathrm{Re}(\lambda_{k+1}),$$

then

$$\begin{aligned} \theta_i = c(\lambda_i) \notin B(0,1), \quad & i = 1, \ldots, k, \\ \theta_i = c(\lambda_i) \in B(0,1), \quad & i = k+1, \ldots, m. \end{aligned}$$

The above corollary suggests a strategy for choosing parameters α_1 et α_2 suitable for accelerating the convergence to $\theta_1 = c(\lambda_1)$. Indeed, α_1 and α_2 may be chosen in such a way that the first unwanted eigenvalue, θ_{k+1} (with $k \geq 1$), is located on the unit circle $B(0,1)$ and that the distance of the dominant eigenvalue $\theta_1 = c(\lambda_1)$ from $B(0,1)$ is maximal. In other words, under the hypothesis of lemma (4.3), we have to maximize $|\theta_1|$ respect to α_1 and α_2 subjected to the constraints

$$\frac{\alpha_1 + \alpha_2}{2} = \mathrm{Re}(\lambda_{k+1}), \quad \alpha_1 < \alpha_2. \tag{31}$$

In the case where λ_1 is real, the following lemma holds (see [19]):

Lemma 4.4 (Garrat, 1991) *Suppose $\lambda_1 \in \mathbb{R}$. Let $1 \leq k < m$ such that $\mathrm{Re}(\lambda_k) < \mathrm{Re}(\lambda_{k+1})$ and $\kappa > 1$ a given real number. If we take*

$$\alpha_1 = \mathrm{Re}(\lambda_{k+1}) - \frac{\kappa+1}{\kappa-1}(\mathrm{Re}(\lambda_{k+1}) - \lambda_1),$$
$$\alpha_2 = \mathrm{Re}(\lambda_{k+1}) + \frac{\kappa+1}{\kappa-1}(\mathrm{Re}(\lambda_{k+1}) - \lambda_1),$$

then

$$\kappa = |\theta_1| \geq |\theta_2| \geq \ldots \geq |\theta_k| > 1 = |\theta_{k+1}| \geq |\theta_i|, \quad i = k+2, \ldots, m.$$

In this case, θ_1 may be made as large as wanted by increasing κ. However, when λ_1 is complex the theory is less satisfactory, we just have the following result (see [19, 20]):

Lemma 4.5 (Garrat, 1991) *Let us suppose that $\lambda_1 = x_1 + iy_1$ with $x_1 < \mathrm{Re}(\lambda_{k+1})$. If*

$$\alpha_1 = \mathrm{Re}(\lambda_{k+1}) - \sqrt{(\mathrm{Re}(\lambda_{k+1}) - x_1)^2 + y_1^2},$$
$$\alpha_2 = \mathrm{Re}(\lambda_{k+1}) + \sqrt{(\mathrm{Re}(\lambda_{k+1}) - x_1)^2 + y_1^2},$$

then the maximum of $|\theta_1|$ subjected to the constraints (31) *is attained. In addition,*

$$|\theta_1| = |\theta_2| = \frac{1}{\sqrt{\xi^2+1} - \xi} > 1, \quad \textit{with} \quad \xi = \frac{\mathrm{Re}(\lambda_{k+1}) - x_1}{|y_1|},$$

and $|\theta_i| \leq 1$ for $i = k+1, \ldots, m$.

The above lemma implies that the extreme character of θ_1 is directly related to the ratio

$$\xi = \frac{\mathrm{Re}(\lambda_{k+1}) - \mathrm{Re}(\lambda_1)}{\mathrm{Im}(\lambda_1)}.$$

The approximation of θ_1 becomes delicate in situations where:

1. $|\,\mathrm{Re}(\lambda_{k+1}) - \mathrm{Re}(\lambda_1)|$ is very small;
2. $|\,\mathrm{Im}(\lambda_1)|$ is very large.

In both cases, the sought eigenvalue θ_1 is very close to the unit circle, which complicates its computation. Indeed, the main difference compared to the case where λ_1 is real comes from the fact that lemma (4.5) does not ensures that θ_1 is a extreme eigenvalue of T_C. We emphasize that this is a direct result of using a rational transformation $\theta = c(\lambda)$, necessary because B is singular.

4.2 Arnoldi's method with implicit restart

The Implicit Restarted Arnoldi Method (IRAM), developed in [41], provides a efficient and numerically stable way for implement a restart, without explicitly computing a new Arnoldi factorization. This method combines the Arnoldi's method [39] with the implicitly shifted QR algorithm [42].

Let us consider a m-step ($m < n$) Arnoldi factorization of a real $n \times n$ non-symmetric matrix A, i.e.

$$AV = VH + re_m^{\mathrm{T}}, \tag{32}$$

in such a way that $V \in \mathbb{R}^{n\times m}$ has m orthonormal columns, $r \in \mathbb{R}^n$ with $V^H r = 0$, and $H \in \mathbb{R}^{m\times m}$ is a upper Hessemberg matrix with non-negative low-diagonal.

A QR type algorithm with explicit shift (see [42]) can be applied to (32). Let $\beta \in \mathbb{R}$ a given shift. We factorize $H - \beta\,\mathrm{I} = QR$, with R upper triangular and Q upper Hessemberg orthogonal. Then, from (32), we get

$$\begin{aligned}
(A - \beta\,\mathrm{I})V - V(H - \beta\,\mathrm{I}) &= re_m^{\mathrm{T}},\\
(A - \beta\,\mathrm{I})V - VQR &= re_m^{\mathrm{T}},\\
(A - \beta\,\mathrm{I})(VQ) - (VQ)(RQ) &= re_m^{\mathrm{T}}Q,\\
A(VQ) - (VQ)(RQ + \beta\,\mathrm{I}) &= re_m^{\mathrm{T}}Q,
\end{aligned} \tag{33}$$

in such a way that setting $V_+ = VQ$ and $H_+ = RQ + \beta \mathrm{I} = Q^{\mathrm{T}} H Q$, we obtain

$$AV_+ = V_+ H_+ + r e_m^{\mathrm{T}} Q.$$

The matrix V_+ has m orthonormal columns (it is the product of V and an orthogonal matrix Q) and H_+ is a upper Hessember matrix (it is a classical property of the QR factorization, see [42]). In addition, the first $m-2$ entries of $e_m^{\mathrm{T}} Q$ are zero. Thus, a new $m-1$ Arnoldi factorization can be obtained by condensing, namely, by equating the first $m-1$ columns of each side:

$$AV_{m-1}^+ = V_{m-1}^+ H_{m-1}^+ + r_{m-1}^+ e_{m-1}^{\mathrm{T}}. \tag{34}$$

Therefore, shifting by β does not disturb the structure of the Arnoldi's factorization. The main result of this operations is that the first column of V_+ has the direction of $(A - \beta \mathrm{I})v_1$, where v_1 is the first column of V. Indeed, by multiplying $(33)_2$ by the canonical vector e_1, we get

$$(A - \beta \mathrm{I})v_1 = V_+ R e_1 = (e_1^{\mathrm{T}} R e_1) V_+ e_1.$$

We can iterate this process by extending the new $(m-1)$-step factorization (34) to a m-step factorization, applying a shift and condensing. The payoff is that each iteration applies to v_1 a linear polynomial in A, and where the root of this polynomial is the applied shift. These ideas can be generalized to the application of p implicit shifts. Starting from a k-step Arnoldi factorization

$$AV_k = V_k H_k + r_k e_k^{\mathrm{T}},$$

we extend this factorization to a $(k+p)$-step Arnoldi factorization

$$AV_{k+p} = V_{k+p} H_{k+p} + r_{k+p} e_{k+p}^{\mathrm{T}}. \tag{35}$$

Then, p implicit shifts $\{\beta_j\}_{j=1}^p$ may be applied to the factorization, resulting in a new factorization

$$AV_{k+p}^+ = V_{k+p}^+ H_{k+p}^+ + r_{k+p} e_{k+p}^{\mathrm{T}} Q,$$

with $V_{k+p}^+ = V_{k+p} Q$, $H_{k+p}^+ = Q^{\mathrm{T}} H_{k+p} Q$ and $Q = Q_1 Q_2 \dots Q_p$, with Q_j the upper Hessemberg orthonormal matrix resulting from the factorization of $H_{h+p} -$

$\beta_j I$ for $j = 1, \ldots, p$. A new k-step Arnoldi factorization can be obtained by equating the first k columns on each side (see [41]):

$$AV_k^+ = V_k^+ H_k^+ + r_k^+ e_k^{\mathrm{T}}. \tag{36}$$

We can iterate applying p steps of the Arnoldi's algorithm to extend the factorization (36) to a new $(k+p)$-factorization (35), then applying shifts and condensing.

As we mentioned above, each implicit application of a shift β_j replaces the initial vector, v_1, by a vector in the direction of $(A - \beta_j \mathrm{I})v_1$. Thus, after application of p implicit shifts we get $v_1 \leftarrow \psi(A)v_1$, where ψ is a p-th degree polynomial with roots $\{\beta_j\}_{j=1}^p$. The choice of the shifts, and hence the construction of the polynomial, is motivated by the fact that if we choose as shifts the eigenvalues that are "unwanted", we can effectively filter the starting vector v_1 so that it will be rich in the direction of the "wanted" eigenvectors. One possible shift selection strategy is the so called "exact shift strategy" (see [41]), where the $(k+p)$ eigenvalues of H_{k+p} are partitioned into a set of k wanted and a set of p unwanted elements. The p unwanted eigenvalues are used as the shifts in the restarting. This is equivalent to restarting the Arnoldi factorization with a linear combination of the approximate eigenvectors associated with the wanted eigenvalues. We notice that the use of implicits shifts of zero (see [34, 30]) is equivalent to performing subspace iteration on V_k.

4.3 Generalized Cayley transform IRAM algorithm

In this paragraph we summarize the algorithm we use for the approximation of the leftmost eigenvalues of (23). This algorithm, fully developed by Lehoucq and Scott in [30], combines shift-invert and generalized Cayley transformations with an IRAM method. Shift-invert is used to get a first approximation of the spectrum and is also used to purify the starting vector and the computed eigenvectors, see [34].

In the sequel k stands for the number of sought-after eigenvalues ($k \ll n$) and $k+p$ ($p > 0$) for the number of computed Arnoldi vectors (i.e. the dimension of the Krylov's subspace). We denote by θ and x the approximate eigenvalues and eigenvectors of T_{SI} and T_C. Hence, $\lambda = c^{-1}(\theta)$ stands for the corresponding approximate eigenvalue of the original problem (23).

The algorithm 1 outlines the Lehoucq and Scott's Generalized Cayley transform IRAM algorithm. In this algorithm, symbol ◊ indicates the steps provided by the ARPACK library (see [30, 32]).

begin
◊ $v_1 \in \mathbb{R}^n$ random unitary vector
purify: $v_1 \leftarrow \mathrm{T}_{SI}(0)v_1$
◊ compute $\theta_1, \ldots, \theta_{k+p}$ from a $(k+p)$-step Arnoldi factorization of T_{SI}
$\lambda_i \leftarrow \dfrac{1}{\theta_i}$, $i = 1, \ldots, k+p$
order λ_i with increasing real parts
◊ $v_1 \in \mathbb{R}^n$ random unitary vector
$v_1 \leftarrow \mathrm{T}_{SI}(0)v_1$
repeat
compute α_1 and α_2 from λ_1 and λ_{k+1} (lemmas 4.4 and 4.5)
◊ compute a $(k+p)$-step Arnoldi factorization of T_C
◊ update v_1 by implicit application of p shifts
◊ compute $\theta_1, \ldots, \theta_{k+p}$ by extension to a $(k+p)$-step factorization
$\lambda_i \leftarrow c^{-1}(\theta_i)$, $i = 1, \ldots, k+p$
order λ_i with increasing real parts
(a) convergence test on θ_i largest in magnitude
until k *converged eigenvalues*
◊ compute eigenvectors x_i corresponding to the converged eigenvalues
obtain eigenvectors of (A, B) by purifying: $x_i \leftarrow \mathrm{T}_{SI}(0)x_i$
end

Algorithm 1. *Cayley transform IRAM algorithm*

4.3.1 Missing eigenvalues

Once the dominant eigenvalues of $\mathrm{T}_C(\alpha_1, \alpha_2)$ are converged, it is necessary to be cautious to avoid eigenvalues which are not of smallest real part. This kind of uncertainty comes from the fact that, unfortunately, the largest eigenvalue of $\mathrm{T}_C(\alpha_1, \alpha_2)$ in magnitude does not necessarily coincide with the leftmost eigenvalues of (23). It is important to notice that there is no theory available to verify whether the left-most eigenvalues have been computed, see [19, 30, 29].

In an attempt to overcome this drawback, in [30], Lehoucq et Scott introduce a additional test on the computed eigenvalues, after step (a) in algorithm 1. Once the dominant eigenvalues (largest in magnitude) of $\mathrm{T}_C(\alpha_1, \alpha_2)$ have acceptable approximations, we order the $k+p$ eigenvalues in decreasing order of their moduli. Then we compute the corresponding eigenvalue approximations of (23) and order them in decreasing order of their real parts. If there is an eigenvalue in the package of the p smallest in magnitude which corresponds to a eigenvalue in the package of the k with smallest real part, we increase the number k of requested eigenvalues. The numerical experiments carried out in [30] showed the effectiveness of this strategy.

4.3.2 Spurious eigenvalues

From lemma 4.1 the generalized Cayley transform maps the infinite eigenvalues of (23) on to $+1$. These eigenvalues are not relevant for the stability analysis but, in practice, are likely to be computed. Indeed, from (30) and since $\alpha_1 < \alpha_2$, if $\theta = 1 + \delta$ with $\delta > 0$ small, then

$$\lambda = c^{-1}(\theta) = \frac{1}{\delta}(\alpha_1(1+\delta) - \alpha_2),$$

become large in magnitude with negative real part. Thus, this eigenvalue could be taken into account in the update of α_1 and α_2. Lehoucq and Scott, in [30], propose that on each iteration all real θ_i which are close to $+1$ must be excluded. They also exclude such spurious eigenvalues when searching for possible missing eigenvalues.

4.3.3 Implicit shifts

We have noticed that the main difficulty in our eigenproblem comes from the existence of infinite eigenvalues. We could try to purify v_1 with the application of implicit shifts of $+1$. Unfortunately, the experiments performed in [30] show that this technique can give bad results. Lehoucq and Spence, in [31], pointed out that the application of shifts corresponding to very good approximations of the eigenvalue can introduce instabilities due to the rounding errors. Lehoucq et Scott in [30] showed that the application of p shifts of 0 give consistently good results. This is equivalent to perform subspace iteration with $\mathrm{T}_C(\alpha_1, \alpha_2)$

on V_k. With this choice the effects of the spurious eigenvalues are strongly attenuated.

4.3.4 Starting Cayley iterations

The information contained in the starting vector is crucial for the performance of the Arnoldi's algorithm. At each Cayley iteration we can improve v_1 by taking into account the information provided by the last iteration. More precisely, we can take v_1 in the invariant subspace associated to the converged eigenvalues. Therefore, see [38], after each Cayley iteration we set

$$v_1 \leftarrow \sum_{i=1}^{l} w_i, \quad v_1 \leftarrow \frac{v_1}{\|v_1\|},$$

where $\{w_i\}_{i=1}^{l}$ stands for a Schur base of the invariant subspace associated to the eigenvalues which have converged in the preceding iteration.

4.4 Matrix-vector product computation

In algorithm 1, each shift-invert purification step or Arnoldi step requires, respectively, a matrix-vector product $\mathrm{y} = \mathrm{T}_{SI}(\alpha_1)\,\mathrm{x}$ or $\mathrm{y} = \mathrm{T}_{C}(\alpha_1, \alpha_2)\,\mathrm{x}$, depending on the transformation in progress. At this point, it is important to provide the following identity

$$\begin{aligned}
\mathrm{T}_C(\alpha_1, \alpha_2) &= (\mathrm{A} - \alpha_1\,\mathrm{B})^{-1}(\mathrm{A} - \alpha_2\,\mathrm{B}) \\
&= (\mathrm{A} - \alpha_1\,\mathrm{B})^{-1}\left[(\mathrm{A} - \alpha_1\,\mathrm{B}) + (\alpha_1 - \alpha_2)\,\mathrm{B}\right] \\
&= \mathrm{I} + (\alpha_1 - \alpha_2)(\mathrm{A} - \alpha_1\,\mathrm{B})^{-1}\,\mathrm{B} \\
&= \mathrm{I} + (\alpha_1 - \alpha_2)\,\mathrm{T}_{SI}(\alpha_1).
\end{aligned}$$

Therefore, on each Arnoldi step or purification step, we have to perform the matrix-vector product $\mathrm{y} = \mathrm{T}_{SI}(\alpha_1)\,\mathrm{x}$. In a equivalent way, we have to solve the following linear system:

$$(\mathrm{A} - \alpha_1\,\mathrm{B})\,\mathrm{y} = \mathrm{B}\,\mathrm{x}\,. \tag{37}$$

In the sequel we will interpret and define a method for the resolution of this system based on the mathematical analysis developed in Part I [16], which can be viewed as a generalized added mass procedure. Let us set

$$\mathrm{x} = \begin{bmatrix} f^{\Omega^{\mathrm{f}}} \\ f^{\Gamma_{\mathrm{out}}} \\ f^{\Gamma_{\mathrm{in}}} \\ f^{\gamma} \\ q \\ h \\ g \end{bmatrix} \in \mathbb{R}^n, \quad \mathrm{y} = \begin{bmatrix} u^{\Omega^{\mathrm{f}}} \\ u^{\Gamma_{\mathrm{out}}} \\ u^{\Gamma_{\mathrm{in}}} \\ u^{\gamma} \\ p \\ z \\ s \end{bmatrix} \in \mathbb{R}^n.$$

After elimination of z by the fifth line of (37), $z = -g - \alpha_1 s$, (37) reduces to

$$\begin{bmatrix} \mathrm{A}_1^{\Omega^{\mathrm{f}}} - \alpha_1 \mathrm{D}_1^{\Omega^{\mathrm{f}}} & \mathrm{A}_1^{\Gamma_{\mathrm{out}}} - \alpha_1 \mathrm{D}_1^{\Gamma_{\mathrm{out}}} & \mathrm{A}_1^{\Gamma_{\mathrm{in}}} - \alpha_1 \mathrm{D}_1^{\Gamma_{\mathrm{in}}} f^{\Gamma_{\mathrm{in}}} & \mathrm{A}_1^{\gamma} - \alpha_1 \mathrm{D}_1^{\gamma} & \mathrm{B}_1 & 0 \\ \mathrm{A}_2^{\Omega^{\mathrm{f}}} - \alpha_1 \mathrm{D}_2^{\Omega^{\mathrm{f}}} & \mathrm{A}_2^{\Gamma_{\mathrm{out}}} - \alpha_1 \mathrm{D}_2^{\Gamma_{\mathrm{out}}} & \mathrm{A}_2^{\Gamma_{\mathrm{in}}} - \alpha_1 \mathrm{D}_2^{\Gamma_{\mathrm{in}}} f^{\Gamma_{\mathrm{in}}} & \mathrm{A}_2^{\gamma} - \alpha_1 \mathrm{D}_2^{\gamma} & \mathrm{B}_2 & 0 \\ 0 & 0 & \mathrm{I} & 0 & 0 & 0 \\ 0 & 0 & 0 & \mathrm{I} & 0 & \alpha_1 \mathrm{G}^0 + \mathrm{G}^1 \\ \mathrm{B}^{\Omega^{\mathrm{f}}} - \alpha_1 \mathrm{E}^{\Omega^{\mathrm{f}}} & \mathrm{B}^{\Gamma_{\mathrm{out}}} - \alpha_1 \mathrm{E}^{\Gamma_{\mathrm{out}}} & \mathrm{B}^{\Gamma_{\mathrm{in}}} - \alpha_1 \mathrm{E}^{\Gamma_{\mathrm{in}}} & \mathrm{B}^{\gamma} - \alpha_1 \mathrm{E}^{\gamma} & \mathrm{C} & 0 \\ \mathrm{F}_a^{\Omega^{\mathrm{f}}} - \alpha_1 \mathrm{F}_d^{\Omega^{\mathrm{f}}} & \mathrm{F}_a^{\Gamma_{\mathrm{out}}} - \alpha_1 \mathrm{F}_d^{\Gamma_{\mathrm{out}}} & \mathrm{F}_a^{\Gamma_{\mathrm{in}}} - \alpha_1 \mathrm{F}_d^{\Gamma_{\mathrm{in}}} & \mathrm{F}_a^{\gamma} - \alpha_1 \mathrm{F}_d^{\gamma} & \mathrm{F}_b & \mathrm{K} + \mathrm{B}^0 + \alpha_1^2 \mathrm{M} \end{bmatrix}$$

$$\times \begin{bmatrix} u^{\Omega^{\mathrm{f}}} \\ u^{\Gamma_{\mathrm{out}}} \\ u^{\Gamma_{\mathrm{in}}} \\ u^{\gamma} \\ p \\ s \end{bmatrix} = \begin{bmatrix} \mathrm{D}_1^{\Omega^{\mathrm{f}}} f^{\Omega^{\mathrm{f}}} + \mathrm{D}_1^{\Gamma_{\mathrm{out}}} f^{\Gamma_{\mathrm{out}}} + \mathrm{D}_1^{\Gamma_{\mathrm{in}}} f^{\Gamma_{\mathrm{in}}} + \mathrm{D}_1^{\gamma} f^{\gamma} \\ \mathrm{D}_2^{\Omega^{\mathrm{f}}} f^{\Omega^{\mathrm{f}}} + \mathrm{D}_2^{\Gamma_{\mathrm{out}}} f^{\Gamma_{\mathrm{out}}} + \mathrm{D}_2^{\Gamma_{\mathrm{in}}} f^{\Gamma_{\mathrm{in}}} + \mathrm{D}_2^{\gamma} f^{\gamma} \\ 0 \\ -\mathrm{G}^0 g \\ \mathrm{E}^{\Omega^{\mathrm{f}}} f^{\Omega^{\mathrm{f}}} + \mathrm{E}^{\Gamma_{\mathrm{out}}} f^{\Gamma_{\mathrm{out}}} + \mathrm{E}^{\Gamma_{\mathrm{in}}} f^{\Gamma_{\mathrm{in}}} + \mathrm{E}^{\gamma} f^{\gamma} \\ \mathrm{F}_d^{\Omega^{\mathrm{f}}} f^{\Omega^{\mathrm{f}}} + \mathrm{F}_d^{\Gamma_{\mathrm{out}}} f^{\Gamma_{\mathrm{out}}} + \mathrm{F}_d^{\Gamma_{\mathrm{in}}} f^{\Gamma_{\mathrm{in}}} + \mathrm{F}_d^{\gamma} f^{\gamma} + \mathrm{M}(h - \alpha_1 g) \end{bmatrix}. \quad (38)$$

As in Section 4.2 of Part I [16] (problem (33) of Part I is the PDE equivalent of (38)) we decompose the solution of the preceding problem as $(u, p) = (u_1, p_1) + (u_2, p_2)$. By block Gaussian elimination of the fluid subproblem, (u_1, p_1) is solution of the first four lines of (38) used with $s = 0$:

$$\begin{bmatrix} \mathrm{A}_1^{\Omega^\mathrm{f}} - \alpha_1 \mathrm{D}_1^{\Omega^\mathrm{f}} & \mathrm{A}_1^{\Gamma_\mathrm{out}} - \alpha_1 \mathrm{D}_1^{\Gamma_\mathrm{out}} & \mathrm{A}_1^{\Gamma_\mathrm{in}} - \alpha_1 \mathrm{D}_1^{\Gamma_\mathrm{in}} f^{\Gamma_\mathrm{in}} & \mathrm{A}_1^{\gamma} - \alpha_1 \mathrm{D}_1^{\gamma} & \mathrm{B}_1 \\ \mathrm{A}_2^{\Omega^\mathrm{f}} - \alpha_1 \mathrm{D}_2^{\Omega^\mathrm{f}} & \mathrm{A}_2^{\Gamma_\mathrm{out}} - \alpha_1 \mathrm{D}_2^{\Gamma_\mathrm{out}} & \mathrm{A}_2^{\Gamma_\mathrm{in}} - \alpha_1 \mathrm{D}_2^{\Gamma_\mathrm{in}} f^{\Gamma_\mathrm{in}} & \mathrm{A}_2^{\gamma} - \alpha_1 \mathrm{D}_2^{\gamma} & \mathrm{B}_2 \\ 0 & 0 & \mathrm{I} & 0 & 0 \\ 0 & 0 & 0 & \mathrm{I} & 0 \\ \mathrm{B}^{\Omega^\mathrm{f}} - \alpha_1 \mathrm{E}^{\Omega^\mathrm{f}} & \mathrm{B}^{\Gamma_\mathrm{out}} - \alpha_1 \mathrm{E}^{\Gamma_\mathrm{out}} & \mathrm{B}^{\Gamma_\mathrm{in}} - \alpha_1 \mathrm{E}^{\Gamma_\mathrm{in}} & \mathrm{B}^{\gamma} - \alpha_1 \mathrm{E}^{\gamma} & \mathrm{C} \end{bmatrix} \begin{bmatrix} u_1^{\Omega^\mathrm{f}} \\ u_1^{\Gamma_\mathrm{out}} \\ u_1^{\Gamma_\mathrm{in}} \\ u_1^{\gamma} \\ p_1 \end{bmatrix}$$

$$= \begin{bmatrix} \mathrm{D}_1^{\Omega^\mathrm{f}} f^{\Omega^\mathrm{f}} + \mathrm{D}_1^{\Gamma_\mathrm{out}} f^{\Gamma_\mathrm{out}} + \mathrm{D}_1^{\Gamma_\mathrm{in}} f^{\Gamma_\mathrm{in}} + \mathrm{D}_1^{\gamma} f^{\gamma} \\ \mathrm{D}_2^{\Omega^\mathrm{f}} f^{\Omega^\mathrm{f}} + \mathrm{D}_2^{\Gamma_\mathrm{out}} f^{\Gamma_\mathrm{out}} + \mathrm{D}_2^{\Gamma_\mathrm{in}} f^{\Gamma_\mathrm{in}} + \mathrm{D}_2^{\gamma} f^{\gamma} \\ 0 \\ -\mathrm{G}^0 g \\ \mathrm{E}^{\Omega^\mathrm{f}} f^{\Omega^\mathrm{f}} + \mathrm{E}^{\Gamma_\mathrm{out}} f^{\Gamma_\mathrm{out}} + \mathrm{E}^{\Gamma_\mathrm{in}} f^{\Gamma_\mathrm{in}} + \mathrm{E}^{\gamma} f^{\gamma} \end{bmatrix}. \quad (39)$$

Similary, we introduce elementary solutions of the first four lines of (38) (fluid subproblem) with unit right hand side

$$\begin{bmatrix} \mathrm{A}_1^{\Omega^\mathrm{f}} - \alpha_1 \mathrm{D}_1^{\Omega^\mathrm{f}} & \mathrm{A}_1^{\Gamma_\mathrm{out}} - \alpha_1 \mathrm{D}_1^{\Gamma_\mathrm{out}} & \mathrm{A}_1^{\Gamma_\mathrm{in}} - \alpha_1 \mathrm{D}_1^{\Gamma_\mathrm{in}} f^{\Gamma_\mathrm{in}} & \mathrm{A}_1^{\gamma} - \alpha_1 \mathrm{D}_1^{\gamma} & \mathrm{B}_1 \\ \mathrm{A}_2^{\Omega^\mathrm{f}} - \alpha_1 \mathrm{D}_2^{\Omega^\mathrm{f}} & \mathrm{A}_2^{\Gamma_\mathrm{out}} - \alpha_1 \mathrm{D}_2^{\Gamma_\mathrm{out}} & \mathrm{A}_2^{\Gamma_\mathrm{in}} - \alpha_1 \mathrm{D}_2^{\Gamma_\mathrm{in}} f^{\Gamma_\mathrm{in}} & \mathrm{A}_2^{\gamma} - \alpha_1 \mathrm{D}_2^{\gamma} & \mathrm{B}_2 \\ 0 & 0 & \mathrm{I} & 0 & 0 \\ 0 & 0 & 0 & \mathrm{I} & 0 \\ \mathrm{B}^{\Omega^\mathrm{f}} - \alpha_1 \mathrm{E}^{\Omega^\mathrm{f}} & \mathrm{B}^{\Gamma_\mathrm{out}} - \alpha_1 \mathrm{E}^{\Gamma_\mathrm{out}} & \mathrm{B}^{\Gamma_\mathrm{in}} - \alpha_1 \mathrm{E}^{\Gamma_\mathrm{in}} & \mathrm{B}^{\gamma} - \alpha_1 \mathrm{E}^{\gamma} & \mathrm{C} \end{bmatrix} \begin{bmatrix} w_j^{\Omega^\mathrm{f}} \\ w_j^{\Gamma_\mathrm{out}} \\ w_j^{\Gamma_\mathrm{in}} \\ w_j^{\gamma} \\ q_j \end{bmatrix}$$

$$= \begin{bmatrix} 0 \\ 0 \\ 0 \\ -(\alpha_1 \mathrm{G}^0 + \mathrm{G}^1) e_j \\ 0 \end{bmatrix}, \quad (40)$$

with e_j the j-th canonical vector of $\mathbb{R}^{n^\mathrm{s}}$.

From the above considerations we propose the following modular resolution for the linear system (37). For α_1 given, we start by factorizing the matrix of (39) or of (40). The solution of the elementary problems (40) and the residual computations

$$\mathrm{F}_{ij}(\alpha_1) = \left[\begin{bmatrix} \mathrm{F}_a^{\Omega^\mathrm{f}} - \alpha_1 \mathrm{F}_d^{\Omega^\mathrm{f}} & \mathrm{F}_a^{\Gamma_\mathrm{out}} - \alpha_1 \mathrm{F}_d^{\Gamma_\mathrm{out}} & \mathrm{F}_a^{\Gamma_\mathrm{in}} - \alpha_1 \mathrm{F}_d^{\Gamma_\mathrm{in}} & \mathrm{F}_a^{\gamma} - \alpha_1 \mathrm{F}_d^{\gamma} & \mathrm{F}_b \end{bmatrix} \begin{bmatrix} w_j^{\Omega^\mathrm{f}} \\ w_j^{\Gamma_\mathrm{out}} \\ w_j^{\Gamma_\mathrm{in}} \\ w_j^{\gamma} \\ q_j \end{bmatrix} \right]_i,$$

with $i, j = 1, \ldots, n^\mathrm{s}$, allow us to compute the n^s columns of the influence matrix $\mathrm{F}(\alpha_1)$, describing the retroaction of the fluid on the structure when the

fluid is set into motion through the structural displacement s. Thus, we can factorize the matrix of the condensed problem, obtained after elimination of (u_2, p_2) in the last line of (38):

$$\mathrm{K} + \mathrm{B}^0 + \mathrm{F}(\alpha_1) + \alpha_1^2\,\mathrm{M}\,.$$

At this level, the computation of (u, p) is immediate. On the one hand, (u_1, p_1) can be obtained by solving (39). Thus, from the residual

$$\mathrm{r} = \begin{bmatrix} \mathrm{F}_a^{\Omega^{\mathrm{f}}} - \alpha_1\,\mathrm{F}_d^{\Omega^{\mathrm{f}}} & \mathrm{F}_a^{\Gamma_{\mathrm{out}}} - \alpha_1\,\mathrm{F}_d^{\Gamma_{\mathrm{out}}} & \mathrm{F}_a^{\Gamma_{\mathrm{in}}} - \alpha_1\,\mathrm{F}_d^{\Gamma_{\mathrm{in}}} & \mathrm{F}_a^{\gamma} - \alpha_1\,\mathrm{F}_d^{\gamma} & \mathrm{F}_b \end{bmatrix} \begin{bmatrix} u_1^{\Omega^{\mathrm{f}}} \\ u_1^{\Gamma_{\mathrm{out}}} \\ u_1^{\Gamma_{\mathrm{in}}} \\ u_1^{\gamma} \\ p_1 \end{bmatrix} - \left[\mathrm{F}_d^{\Omega^{\mathrm{f}}} f^{\Omega^{\mathrm{f}}} + \mathrm{F}_d^{\Gamma_{\mathrm{out}}} f^{\Gamma_{\mathrm{out}}} + \mathrm{F}_d^{\Gamma_{\mathrm{in}}} f^{\Gamma_{\mathrm{in}}} + \mathrm{F}_d^{\gamma} f^{\gamma} \right],$$

we obtain the fluid load at the interface. By solving the condensed problem

$$\left(\mathrm{K} + \mathrm{B}^0 + \mathrm{F}(\alpha_1) + \alpha_1^2\,\mathrm{M}\right) s = -\,\mathrm{r} + \mathrm{M}(h - \alpha_1 g), \tag{41}$$

we get s. Once s is computed, we obtain (u_2, p_2) from

$$(u_2, p_2) = \sum_{j=1}^{n^{\mathrm{s}}} s_j (w_j, q_j),$$

and then with (u_1, p_1) we finally compute (u, p) .

Clearly, we could separately build the matrices A and B and then factorize $\mathrm{A} - \alpha_1\,\mathrm{B}$. However, this would imply, on the one hand, a larger cost of factorization, and on the other hand, a loss in the modular character of the solution. It is well known that the modularity of an algorithm implies reliability and robustness. In the numerical experiments reported in section 5, the numerical resolution of the linear systems resulting from the fluid subproblems is performed using the UMFPACK package (available for download on `www.netlib.org/linalg`). This package implements an hybrid algorithm unifrontal/multifrontal for the direct resolution of sparse linear systems, see [11]. The resolution of the condensed problem (41), of small size, is realized using a standard LU factorization, as implement in the LAPACK library (available for download on `www.netlib.org/lapack`).

In the next section we will point out the performance of algorithm 1 for the computation of the leftmost eigenvalues of (23), when performing the matrix vector multiplication as described above.

5 Numerical experiments

In this section we report the numerical results obtained in three significant two-dimensional test cases. Of course, three-dimensional experiments can be addressed with our approach, by providing the corresponding linearized fluid solver.

These numerical experiments will allow us to point out, on the one hand, the performance of the proposed discretization scheme (17) and, on the other hand, the efficiency of the linearization-transpiration approach developed in Part I [16]. In the following paragraphs we compare our numerical results to former approaches and to experimental data coming from wind-tunnel experiments.

5.1 Structure placed in a viscous flow at rest

In this paragraph we will consider the stability problem of a rigid tube immersed in a incompressible viscous fluid at rest. The fluid is contained in a three-dimensional cavity containing the tube. It is assumed that the tube is elastically mounted (with stiffness $k > 0$) in such a way that it can only vibrate in a transverse plane perpendicular to the tube. Moreover, axial effects are not considered. Then, the problem is studied in two dimensions restricting it to any of the sections, Ω, of the cavity that are perpendicular to the tube, see figure 2. In the sequel Ω^{f} stands for the domain section occupied by the fluid, Ω^{s} for the transversal section of the tube, γ for the section of the fluid-structure interface, and $\Gamma = \partial\Omega$ for the section of the cavity boundary.

We assume that the fluid and the structure are at equilibrium in this configuration. Since the fluid is at rest, we have $u_0 = 0$ and $p_0 = 0$. Therefore, eigenproblem (3) reduces to (see also [16, Section 4.1.1]): find $\lambda \in \mathbb{C}$, $u : \Omega^{\mathrm{f}} \longrightarrow \mathbb{C}^2$, $p : \Omega^{\mathrm{f}} \longrightarrow \mathbb{C}$ and $s \in \mathbb{C}^{n^{\mathrm{s}}}$, with $\displaystyle\int_{\Omega^{\mathrm{f}}} p \,\mathrm{d}x = 0$ and $(u, p, s) \neq 0$,

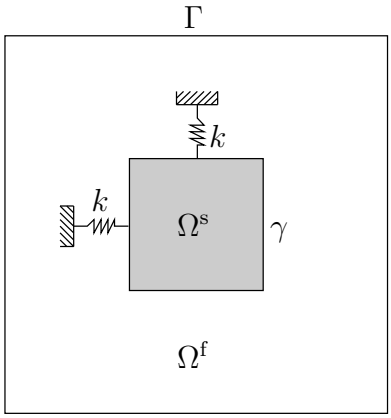

Figure 2: The section Ω

such that

$$\begin{aligned} -2\nu \operatorname{div} \varepsilon(u) + \frac{1}{\rho}\nabla p &= \lambda u, \quad \text{in} \quad \Omega^{\mathrm{f}}, \\ \operatorname{div} u &= 0, \quad \text{in} \quad \Omega^{\mathrm{f}}, \\ u &= 0, \quad \text{on} \quad \Gamma, \\ u &= -\lambda s, \quad \text{on} \quad \gamma, \\ \lambda^2 m s + k s &= -\int_\gamma \sigma(u,p) n \, \mathrm{d}a. \end{aligned} \tag{42}$$

Here, $m > 0$ is the mass of the tube.

This model problem, coupling the Stokes equations with those of a rigid body in translation, was already proposed and studied in [8], for the determination of the vibration frequencies of a tube rack immersed in a viscous fluid at rest, see also [9]:

Theorem 5.1 (Conca, Durán & Planchard, 1992) *The spectrum of* (42) *consists of a countable infinite quantity of complex numbers which converge to infinity. Moreover, the eigenvalues have the following properties:*

1. $\mathrm{Re}(\lambda_i) > 0, \quad \forall i \geq 1;$
2. *There exists at most four eigenvalues with non-zero imaginary part;*

3. If $\mathrm{Im}(\lambda) \neq 0$, *then*

$$|\lambda| \leq \sqrt{\frac{k}{m}}.$$

A numerical study of problem (42) was carried out in [7]. The problem was approximated with a $\mathbb{P}_2/\mathbb{P}_1$ finite element discretization of the Stokes equations. The numerical experiments obtained then corroborate the results of theorem 5.1.

Theorem 5.1 ensures that the eigenvalues of (42) have positive real part. Therefore, the steady equilibrium in which the fluid and structure are at rest is linearly stable, namely, the vibrations of the tube are damped by the fluid viscosity.

In order to validate the discretization scheme (17) and the algorithm 1, we have taken again the numerical experiments reported by Conca and Durán in [7]. Our numerical experiments were performed keeping the same geometry: a closed cavity $\Omega = (-3,3) \times (-3,3)$ with a perforation $\Omega^{\mathrm{s}} = (-1,1) \times (-1,1)$, and using $\mathbb{P}_1/\mathbb{P}_1$ finite elements.

To discretize the fluid domain $\Omega^{\mathrm{f}} = \Omega - \overline{\Omega}^{\mathrm{s}}$, we have considered four triangulations represented in figure 3. As in [7], the density ρ, the kinematic viscosity ν and the mass of the tube m were fixed to 1. For each triangulation, the left-most eigenvalues of (23) were approximated for several values of k: 0.01, 0.1, 1, 10 and 100. The number of requested eigenvalues was fixed to 10 and the dimension of the Krylov subspace to 30. Finally, the tolerance for the Ritz estimates was 10^{-6} (see [30]). On the finer grid, figure 3(d), the computations took in average two iterations of Cayley and 4 minutes of CPU time on a HP Visualize 8200 workstation. In addition, the relative residuals $\| \mathrm{A}\,\mathrm{x} - \lambda\,\mathrm{B}\,\mathrm{x} \|$, with $\| \mathrm{x} \| = 1$, was between 10^{-7} and 10^{-15}

It is important to notice that, in [7], the authors have computed all the eigenvalues of the discretized problem, that was done with the payoff of using very coarse meshes. In figures 4 to 8 we report, for each value of k, the real part of the computed leftmost eigenvalue as a function of the mesh step h. The dashed line represents the more accurate value provided in [7], it corresponds to a 128 triangles mesh. We can notice (for small h) a linear convergence of the approximations and a good agreement of both numerical results.

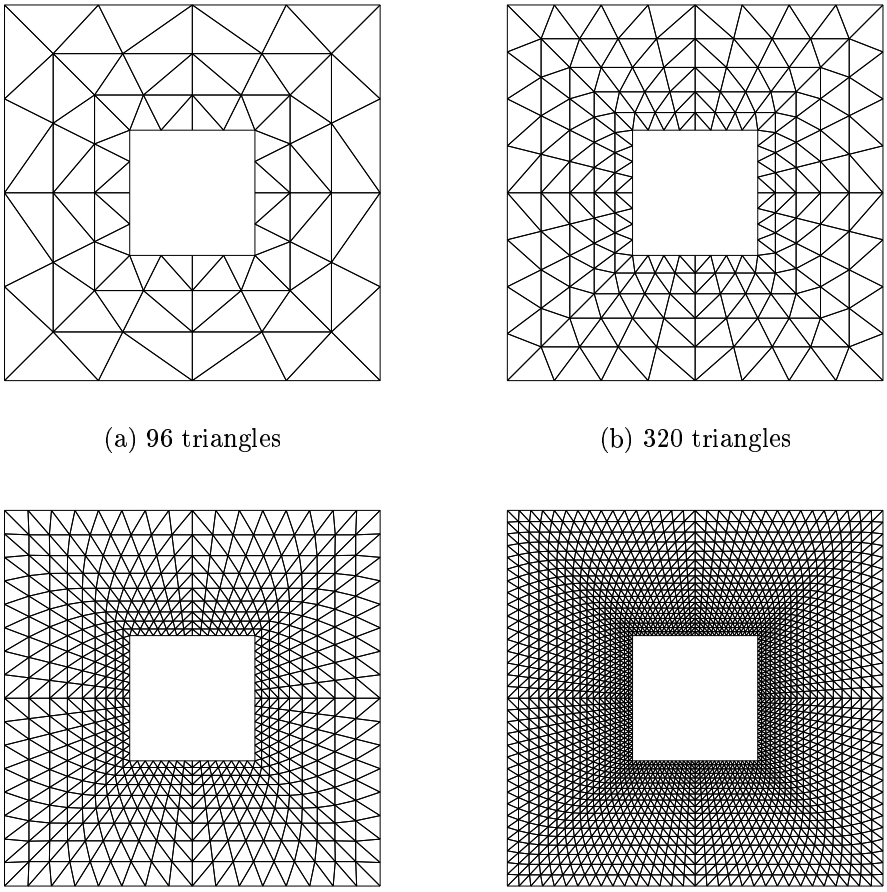

(a) 96 triangles

(b) 320 triangles

(c) 1152 triangles

(d) 4608 triangles

Figure 3: Triangulations of the fluid domain Ω^{f}

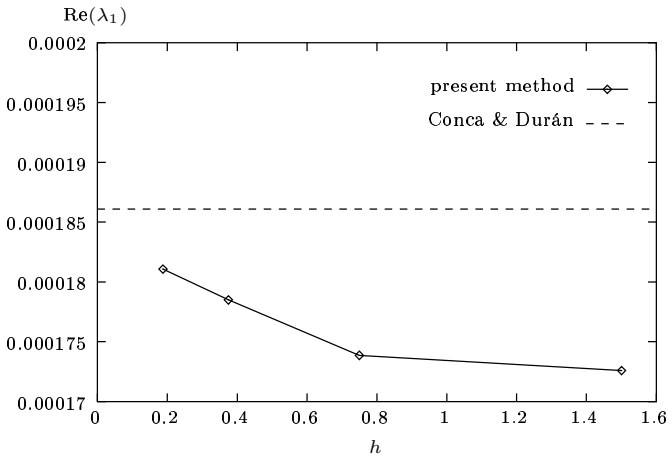

Figure 4: Approximations of $\mathrm{Re}(\lambda_1)$ for $k = 0.01$

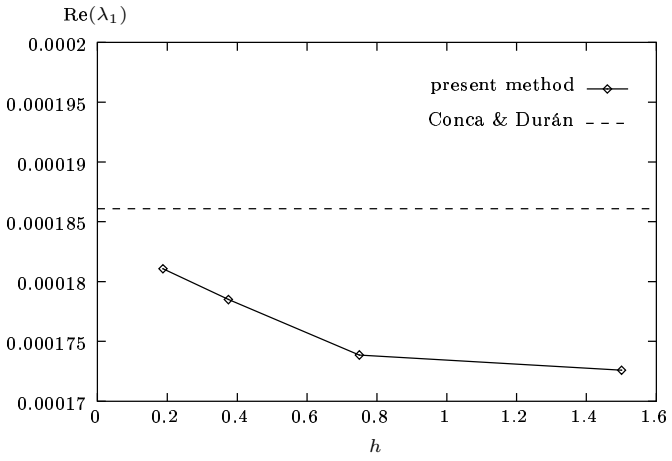

Figure 5: Approximations of $\mathrm{Re}(\lambda_1)$ for $k = 0.1$

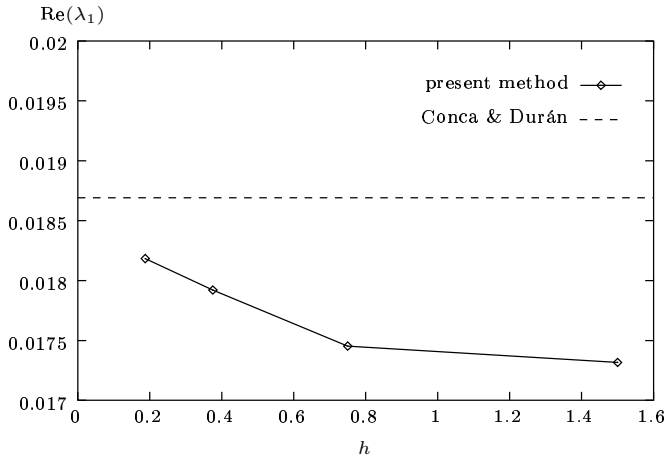

Figure 6: Approximations of $\mathrm{Re}(\lambda_1)$ for $k = 1$

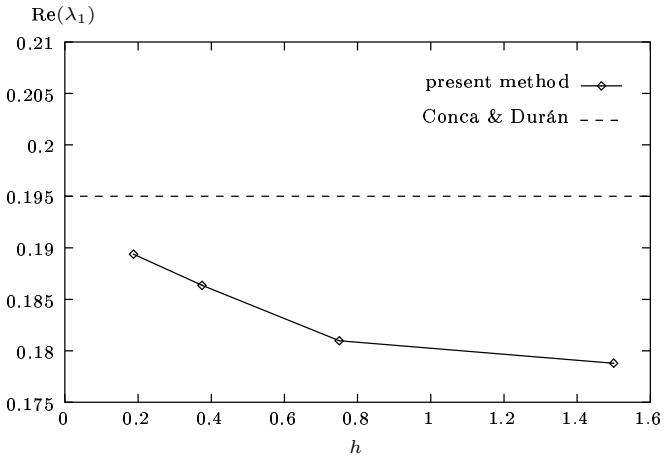

Figure 7: Approximations of $\mathrm{Re}(\lambda_1)$ for $k = 10$

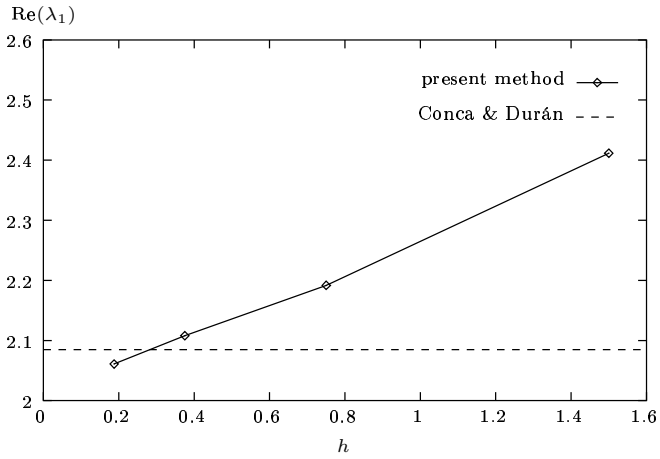

Figure 8: Approximations of $\mathrm{Re}(\lambda_1)$ for $k = 100$

In table 1 we have reported the 10 leftmost eigenvalues corresponding to our finer grid (figure 3(d)). On the other hand, table 2 provides the eigenvalues obtained in [7] with a 128 triangles mesh.

We can immediately point out the good agreement of these results. In both cases the number of complex eigenvalues is not higher than 4, which was predicted by theorem 5.1. In addition, both spectra show a similar behavior when k varies. In particular, for small values of the parameter k the spectra are made up only of real numbers, and when k increases complex eigenvalues appear.

In figures 9 to 13 we present the velocity field and the isobaric lines corresponding to eigenvectors associated with some eigenvalues of table 1. These figures agree perfectly with those provided in [7]. A noticeable feature, already observed in [7], lies in the fact that the simple eigenvalues of large magnitude are insensitive to variations of k. In other words, they are purely fluid eigenmotions. This phenomenon can be easily noted in figures 10, 12 and 13. Here, the coupled eigenmotions do not correspond to a displacement on the tube. We recall that $u = \lambda s$ on the interface.

$k = 0.01$	$k = 0.1$	$k = 1$	$k = 10$	$k = 100$
1.810×10^{-4}	1.811×10^{-3}	1.818×10^{-2}	1.894×10^{-1}	$2.061+1.696i$
1.810×10^{-4}	1.811×10^{-3}	1.818×10^{-2}	1.894×10^{-1}	$2.061-1.696i$
2.651	2.651	2.651	2.651	$2.061+1.696i$
3.870	3.869	3.855	3.707	$2.061-1.696i$
3.870	3.869	3.855	3.707	2.651
8.152	8.152	8.152	8.152	8.152
8.238	8.238	8.238	8.238	8.238
8.382	8.382	8.381	8.379	8.361
8.382	8.382	8.381	8.379	8.361
9.218	9.218	9.218	9.218	9.218

Table 1: The 10 leftmost eigenvalues with the grid 3(d)

$k = 0.01$	$k = 0.1$	$k = 1$	$k = 10$	$k = 100$
1.868×10^{-4}	1.869×10^{-3}	1.876×10^{-2}	1.960×10^{-1}	$2.067+1.752i$
1.868×10^{-4}	1.869×10^{-3}	1.876×10^{-2}	1.960×10^{-1}	$2.067-1.752i$
2.625	2.625	2.625	2.625	$2.067+1.752i$
3.863	3.862	3.847	3.696	$2.067-1.752i$
3.863	3.862	3.847	3.696	2.625
7.909	7.909	7.909	7.909	7.909
7.934	7.934	7.934	7.934	7.934
8.167	8.167	8.167	8.164	8.138
8.167	8.167	8.167	8.164	8.138
9.223	9.223	9.223	9.223	9.223

Table 2: The 10 leftmost eigenvalues reported in [7]

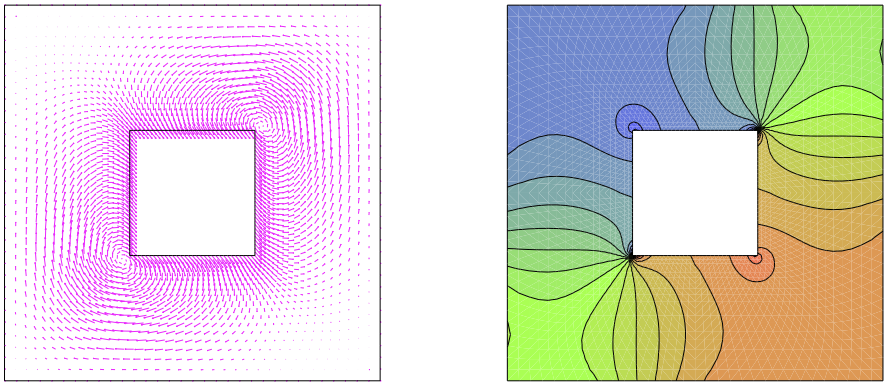

(a) Velocity field (b) Isobaric lines

Figure 9: Eigenvalue $\lambda_1 = 1.818 \times 10^{-2}$

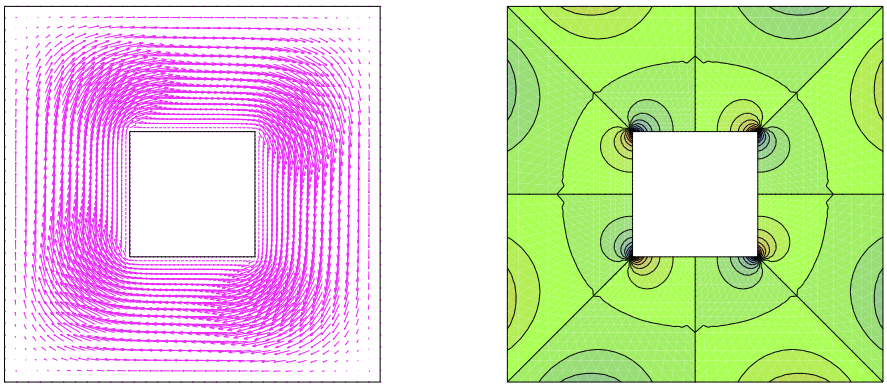

(a) Velocity field (b) Isobaric lines

Figure 10: Eigenvalue $\lambda_3 = 2.651$

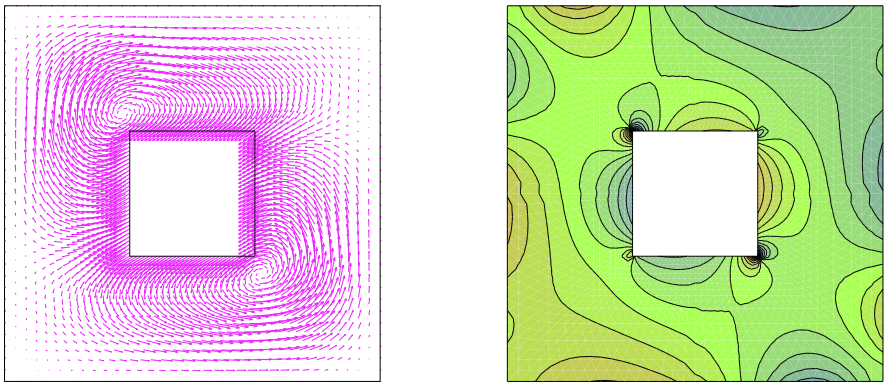

(a) Velocity field (b) Isobaric lines

Figure 11: Eigenvalue $\lambda_4 = 3.855$

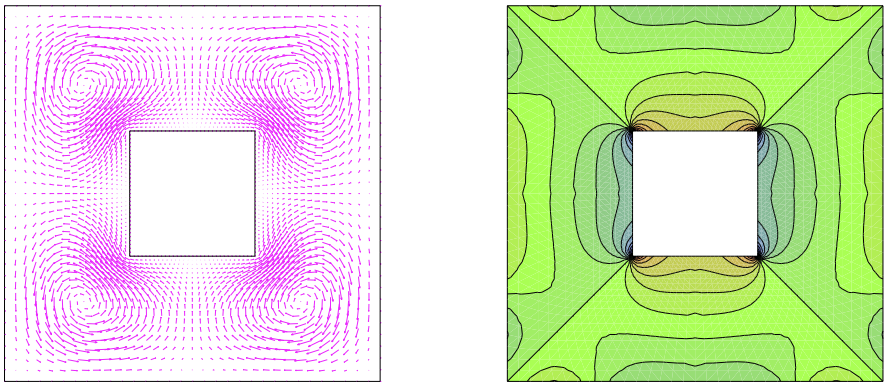

(a) Velocity field (b) Isobaric lines

Figure 12: Eigenvalue $\lambda_6 = 8.152$

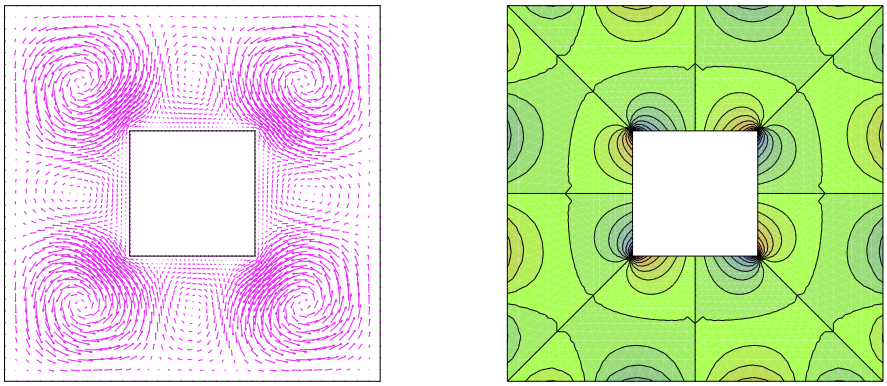

(a) Velocity field (b) Isobaric lines

Figure 13: Eigenvalue $\lambda_7 = 8.238$

5.2 Cantilever pipe conveying a fluid

In this paragraph we address the problem of the linear stability of a cantilever pipe conveying a fluid, see figure 14. It is well known, see [35, 37], that this fluid-structure system loses stability for high flow velocities by flutter.

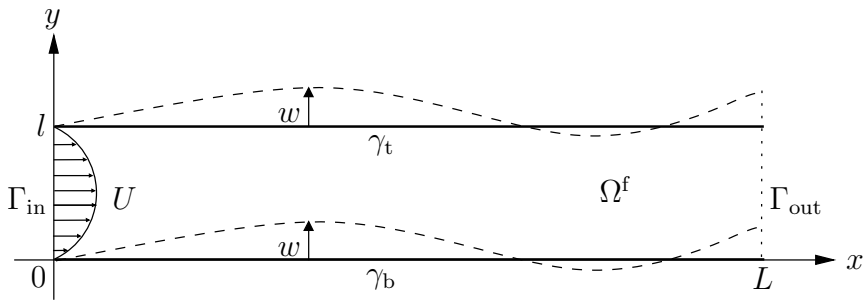

Figure 14: Cantilever pipe conveying a fluid

Païdoussis, in [35], derives a simplified linear model for the motion of the pipe by adding fluid forces to the pipe structural equations, the pipe being

treated as a beam, modeled as (see [27])

$$\begin{aligned} EI\frac{\partial^4 w}{\partial x^4} + m\ddot{w} = f, \quad \text{in} \quad (0,L), \\ w = \frac{\partial w}{\partial x} = 0, \quad \text{on} \quad x = 0, \\ \frac{\partial^2 w}{\partial x^2} = \frac{\partial^3 w}{\partial x^3} = 0, \quad \text{on} \quad x = L, \end{aligned} \tag{43}$$

where w stands for the flexural displacement, E for the Young's modulus, I for the inertia momentum, m for the mass per unit length, L for the pipe length and f for the transverse load applied on the pipe per unit length. In [35], Païdoussis provides the following expression for f:

$$f = M\ddot{w} + 2MU\frac{\partial \dot{w}}{\partial x} + MU^2\frac{\partial^2 w}{\partial x^2}.$$

Here, M represents the mass per unit length of the fluid and U the mean axial velocity of the internal flow. Hence, substituting the above expression in (43), we get that the flexural motion of the pipe under the flow effects can be modeled by the following linear equation:

$$EI\frac{\partial^4 w}{\partial x^4} + 2MU\frac{\partial \dot{w}}{\partial x} + MU^2\frac{\partial^2 w}{\partial x^2} + (M+m)\ddot{w} = 0, \quad \text{in} \quad (0,L), \tag{44}$$

provided with the boundary conditions $(43)_{2,3}$. Païdoussis analyzes the stability of the coupled system by computing the harmonic solutions of (44). More precisely, setting $w(x,t) = w(x)e^{-\lambda t}$ with $\lambda \in \mathbb{C}$, we obtain, from (44), the following quadratic eigenproblem:

$$EI\frac{\partial^4 w}{\partial x^4} - 2\lambda MU\frac{\partial w}{\partial x} + MU^2\frac{\partial^2 w}{\partial x^2} + \lambda^2(M+m)w = 0, \quad \text{in} \quad (0,L).$$

In [35], the solutions of the above eigenproblem are approximated by computing the eigenvalues of the algebraic system resulting from the projection of equation (44) on the first eigenmodes of the beam.

In [37], a similar approach was used for the stability analysis of the coupled system. Again, it is assumed that the pipe walls vibrate with beam modes. Then, by projecting equation $(43)_1$ on the first n^{s} beam eigenmodes we obtain

$$\mathrm{M}\,\ddot{s} + \mathrm{C}\,\dot{s} + \mathrm{K}\,s = f_g, \tag{45}$$

with M and K the $n^s \times n^s$ matrices of mass and stiffness and $s, f_g \in \mathbb{R}^{n^s}$ the vectors of generalized displacements and fluid loads on the interface, respectively. The numerical computations reported in [37] are based on the assumption that these fluid loads at the fluid-structure interface, f_g, can be expressed in terms of added mass, added damping and added stiffness, i.e.

$$f_g = -\,\mathrm{M}_a\,\ddot{s} - \mathrm{C}_a\,\dot{s} - \mathrm{K}_a\,s, \tag{46}$$

where M_a, C_a and K_a stand, respectively, for the $n^s \times n^s$ full matrices of added mass, damping, and stiffness. The above temporal decomposition of the fluid loads is not really exact. Indeed, even for small oscillations, the non-linear character of the fluid introduces a dependence of the added mass and damping matrices with respect to the frequency of the motion. The added matrices M_a, C_a and K_a are classically obtained using the forced oscillation method, see [37, 46, 47]. The structure is subjected to a forced sinusoidal oscillation and the above added matrices are computed by measuring the resulting fluid interface load over a fixed number of periods. In [37] this is done numerically from the solution of the incompressible Navier-Stokes equations, where the interface motion is taken into account via transpiration boundary conditions (see [37, 14]). It is noticed, in [37], that these fluid computations become very expensive when dealing with high frequency oscillations (130 minutes of computing time for three oscillation periods).

Once the above added matrices have been computed, equation (45) can be rewritten as

$$(\mathrm{M}+\mathrm{M}_a)\ddot{s} + \mathrm{C}_a\,\dot{s} + (\mathrm{K}+\mathrm{K}_a)s = 0. \tag{47}$$

Thus, the stability analysis can be carried out by computing its harmonic solutions, $s(t) = se^{-\lambda t}$ with $s \in \mathbb{C}^{n^s}$ and $\lambda \in \mathbb{C}$. Equivalently, we can compute the roots of the following characteristic polynomial:

$$\det\left(\lambda^2(\mathrm{M}+\mathrm{M}_a) - \lambda\,\mathrm{C}_a + (\mathrm{K}+\mathrm{K}_a)\right) = 0.$$

In this paragraph we intend to reproduce the main stability predictions obtained by Païdoussis and Renou in [35, 37], using the linearization-transpiration approach developed in Part I [16]. For the sake of simplicity, and following [37],

we will couple the flow into the pipe with the first three modes of a cantilever beam modeling the pipe walls.

In the sequel we will deal with a cantilever pipe of length L and width l, conveying an homogeneous incompressible viscous fluid of density ρ and kinematic viscosity ν, see the figure 14. Let us consider the following parabolic velocity profile on the inlet boundary $\Gamma_{\rm in}$:

$$u_{\Gamma_{\rm in}}(y) = 6U\frac{y}{l}\left(1-\frac{y}{l}\right), \quad y \in [0,l],$$

where U stands for the mean velocity of the flow. The coupled fluid-structure system exhibits a steady equilibrium state (u_0, p_0, s_0) satisfying equations (1) and (2), i.e.

$$\begin{aligned}
\nabla u_0 u_0 - 2\nu \,\mathrm{div}\,\varepsilon(u_0) + \frac{1}{\rho}\nabla p_0, &\quad \text{in} \quad \Omega^{\rm f},\\
\mathrm{div}\, u_0 = 0, &\quad \text{in} \quad \Omega^{\rm f},\\
u_0 = u_{\Gamma_{\rm in}}, &\quad \text{on} \quad \Gamma_{\rm in},\\
\sigma(u_0,p_0)n = 0, &\quad \text{on} \quad \Gamma_{\rm out},\\
u_0 = 0, &\quad \text{on} \quad \gamma_{\rm t}\cup\gamma_{\rm b},\\
\mathrm{K}\, s_0 = -\int_{\gamma_{\rm t}\cup\gamma_{\rm b}} \Phi^{\rm T}\sigma(u_0,p_0)n \,\mathrm{d}a.&
\end{aligned} \tag{48}$$

Remark 5.2 *For a symmetric velocity profile (respect to the pipe axis) the fluid load is opposite on the walls. Therefore, the resultant*

$$\int_{\gamma_{\rm t}\cup\gamma_{\rm b}} \Phi^{\rm T}\sigma(u_0,p_0)n \,\mathrm{d}a = 0,$$

and then $s_0 = 0$. In this case the fluid domain $\Omega^{\rm f}$ at the equilibrium is known.

The stability analysis of this equilibrium state can be carried out using the linearization-transpiration framework introduced in Part I [16]. Hence, the study of the linear stability of (u_0, p_0, s_0) reduces to the approximation of the leftmost eigenvalues of problem (3), i.e.: find $\lambda \in \mathbb{C}$, $u : \Omega^{\rm f} \longrightarrow \mathbb{C}^2$,

Figure 15: Mesh of the fluid domain Ω^{f} at equilibrium

$p : \Omega^{\mathrm{f}} \longrightarrow \mathbb{C}$ and $s \in \mathbb{C}^{n^{\mathrm{s}}}$, with $(u, p, s) \neq 0$, such that

$$\begin{aligned}
\nabla u_0 u + \nabla u u_0 - 2\nu \operatorname{div} \varepsilon(u) + \frac{1}{\rho}\nabla p = \lambda u, \quad & \text{in} \quad \Omega^{\mathrm{f}}, \\
\operatorname{div} u = 0, \quad & \text{in} \quad \Omega^{\mathrm{f}}, \\
u = 0, \quad & \text{on} \quad \Gamma_{\mathrm{in}}, \\
\sigma(u,p)n = -\nabla\sigma(u_0,p_0)\Phi s n, \quad & \text{on} \quad \Gamma_{\mathrm{out}}, \\
u = -\lambda\Phi s - \nabla u_0 \Phi s, \quad & \text{on} \quad \gamma_{\mathrm{t}} \cup \gamma_{\mathrm{b}}, \\
\lambda^2 \mathrm{M}\, s + \left(\mathrm{K} + \mathrm{B}^0\right) s = -\int_{\gamma_{\mathrm{t}}\cup\gamma_{\mathrm{b}}} \Phi^{\mathrm{T}} \sigma(u,p) n \, \mathrm{d}a. &
\end{aligned} \tag{49}$$

Remark 5.3 *In this specific case, the outlet boundary Γ_{out} is mobile. Therefore, we must impose a "transpiration" boundary condition which takes into account the transport term $\nabla\sigma(u_0,p_0)\Phi s n$, coming from the linearization of the "do nothing" boundary condition in the perturbed problem (see Part I [16]).*

Using the discretization scheme (17) the above eigenproblem becomes a generalized eigenvalue problem of type (23). Its leftmost eigenvalues can be approximated using algorithm 1. In our numerical computations we have chosen the following data, reported in [37]:

$$\begin{aligned}
L &= 1 \text{ m}, & m &= 160 \text{ Kg/m}^2, \\
E &= 1.5 \times 10^9 \text{ Pa}, & \rho &= 1000 \text{ Kg/m}^3, \\
l &= 0.04 \text{ m}, & M &= 40 \text{ Kg/m}^2, \\
I &= 1.0053 \times 10^{-8} \text{ m}^4, & \nu &= 5 \times 10^{-5} \text{ m}^2/\text{s}.
\end{aligned}$$

As in many studies of Païdoussis [35], the above mass values correspond to a mass ratio $\beta = M/(M+m)$ of 0.2. In addition, the mean velocity U (in m/s) took the following values: 0, 0.614, 1.228, 1.842, 2.456, 3.07 and 3.684.

The fluid domain inside the pipe was discretized using a 4000 triangles mesh, see figure 15. For each value of U we compute the fluid state at equilibrium (u_0, p_0) using a $\mathbb{P}_2/\mathbb{P}_1$ Navier-Stokes solver (see figure 16).

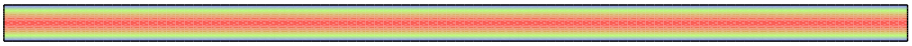

Figure 16: Velocity magnitude at the reference equilibrium for $U = 3.684$ m/s

Remark 5.4 *Since the fluid computation are carried out using a* $\mathbb{P}_2/\mathbb{P}_1$ *discretization of* (48)*, we can define a first explicit approximation of the added stiffness matrix* B^0 *defined in* (4)*.*

In algorithm 1 the number of requested eigenvalues was fixed to 6, the dimension of the Krylov subspace to 20 and the Ritz estimates tolerance to 10^{-6}. For each value of U, the mean computational time was 3 minutes on a HP Visualize 8200 workstation with 3 Cayley iterations.

In tables 3 to 9 we have reported, for each value of U, the first smallest real part eigenvalues and the corresponding residuals. This results point out the sensitivity of the approximations of the imaginary part. This phenomenon was already announced in paragraph 4.1, see also [30, 19]. Indeed, the eigenvalues of (23) with large imaginary parts are mapped to eigenvalues of T_C close to the unit circle, which are difficult to approximate.

λ	$\|\mathrm{A}\,\mathrm{x}-\lambda\,\mathrm{B}\,\mathrm{x}\|$
$1.371 \times 10^{-3} + 9.662 \times 10^{-1} i$	3.560×10^{-15}
$1.371 \times 10^{-3} - 9.662 \times 10^{-1} i$	3.560×10^{-15}
$7.945 \times 10^{-3} + 6.069 i$	5.063×10^{-11}
$7.945 \times 10^{-3} - 6.069 i$	5.063×10^{-11}
$1.966 \times 10^{-2} + 17.01 i$	6.284×10^{-7}
$1.966 \times 10^{-2} - 17.01 i$	6.284×10^{-7}

Table 3: Eigenvalues and residuals for $U = 0$ m/s

λ	$\|\mathrm{A}\,\mathrm{x}-\lambda\,\mathrm{B}\,\mathrm{x}\|$
$1.907\times10^{-1}+16.93i$	1.241×10^{-8}
$1.907\times10^{-1}-16.93i$	1.241×10^{-8}
$2.060\times10^{-1}+5.988i$	1.164×10^{-10}
$2.060\times10^{-1}-5.988i$	1.164×10^{-10}
$2.392\times10^{-1}+9.718\times10^{-1}i$	2.435×10^{-12}
$2.392\times10^{-1}-9.718\times10^{-1}i$	2.435×10^{-12}

Table 4: Eigenvalues and residuals for $U = 0.614$ m/s

λ	$\|\mathrm{A}\,\mathrm{x}-\lambda\,\mathrm{B}\,\mathrm{x}\|$
$3.713\times10^{-1}+16.67i$	1.377×10^{-5}
$3.713\times10^{-1}-16.67i$	1.377×10^{-5}
$3.854\times10^{-1}+5.698i$	4.279×10^{-9}
$3.854\times10^{-1}-5.698i$	4.279×10^{-9}
$5.067\times10^{-1}+9.871\times10^{-1}i$	3.942×10^{-11}
$5.067\times10^{-1}-9.871\times10^{-1}i$	3.942×10^{-11}

Table 5: Eigenvalues and residuals for $U = 1.228$ m/s

λ	$\|\mathrm{A}\,\mathrm{x}-\lambda\,\mathrm{B}\,\mathrm{x}\|$
$4.829\times10^{-1}+5.191i$	5.889×10^{-13}
$4.829\times10^{-1}-5.191i$	5.889×10^{-13}
$5.304\times10^{-1}+16.17i$	2.097×10^{-6}
$5.304\times10^{-1}-16.17i$	2.097×10^{-6}
$8.627\times10^{-1}+1.067i$	1.631×10^{-13}
$8.627\times10^{-1}-1.067i$	1.631×10^{-13}

Table 6: Eigenvalues and residuals for $U = 1.842$ m/s

λ	$\|\,\mathrm{A}\,\mathrm{x}-\lambda\,\mathrm{B}\,\mathrm{x}\,\|$
$3.220\times10^{-1}+4.476i$	6.652×10^{-14}
$3.220\times10^{-1}-4.476i$	6.652×10^{-14}
$6.577\times10^{-1}+15.43i$	4.131×10^{-8}
$6.577\times10^{-1}-15.43i$	4.131×10^{-8}
$1.495+1.288i$	1.643×10^{-14}
$1.495-1.288i$	1.643×10^{-14}

Table 7: Eigenvalues and residuals for $U = 2.456$ m/s

λ	$\|\,\mathrm{A}\,\mathrm{x}-\lambda\,\mathrm{B}\,\mathrm{x}\,\|$
$-3.477\times10^{-1}+4.000i$	2.709×10^{-14}
$-3.477\times10^{-1}-4.000i$	2.709×10^{-14}
$7.243\times10^{-1}+14.39i$	1.731×10^{-10}
$7.243\times10^{-1}-14.39i$	1.731×10^{-10}
$2.675+1.295i$	2.205×10^{-14}
$2.675-1.295i$	2.205×10^{-14}

Table 8: Eigenvalues and residuals for $U = 3.070$ m/s

λ	$\|\,\mathrm{A\,x}-\lambda\,\mathrm{B\,x}\,\|$
$-1.026+4.181i$	6.751×10^{-15}
$-1.026-4.181i$	6.751×10^{-15}
$6.633\times10^{-1}+12.93i$	1.270×10^{-12}
$6.633\times10^{-1}-12.93i$	1.270×10^{-12}
$3.930+6.927\times10^{-1}i$	1.636×10^{-14}
$3.930-6.927\times10^{-1}i$	1.636×10^{-14}

Table 9: Eigenvalues and residuals for $U = 3.684$ m/s

The leftmost eigenvalues, namely, the smallest damping provided by our numerical computations are compared to those obtained by Païdoussis and Renou [35, 37] in figure 17. We can notice the good agreement of our computations and those of Renou. These values are a little lower than those of the Païdoussis model. However, all this curves give comparable stability results. A flutter instability is predicted in the range of flow velocities $U \in [2.5, 3.5]$. Figure 17 shows a typical situation of flutter instability. Indeed, if the velocity of the flow is augmented gradually the damping of the oscillations increases. However, with further increase in the flow velocity, a point is reached from where the damping of the system decreases again, down to negative (unstable) values.

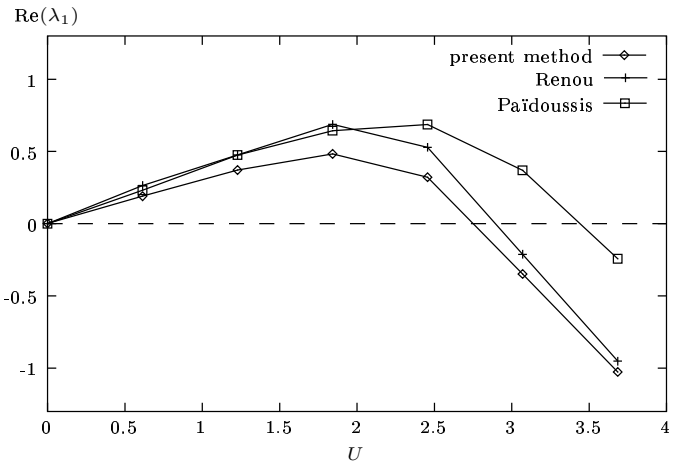

Figure 17: Real part of the leftmost eigenvalue: damping

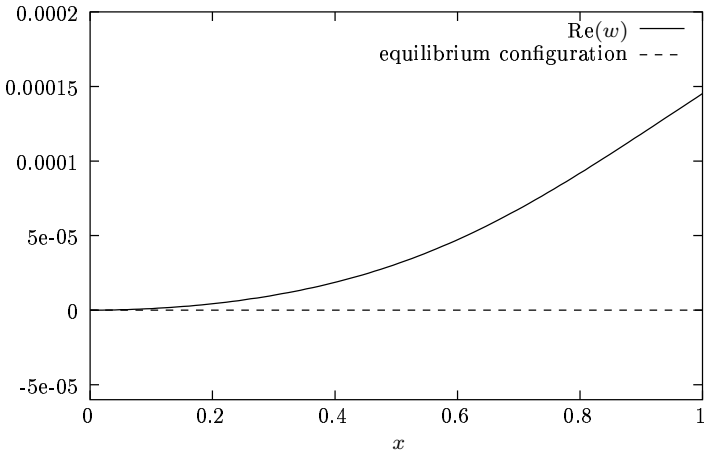

Figure 18: Real part of the displacement in the unstable mode for $U = 3.070$

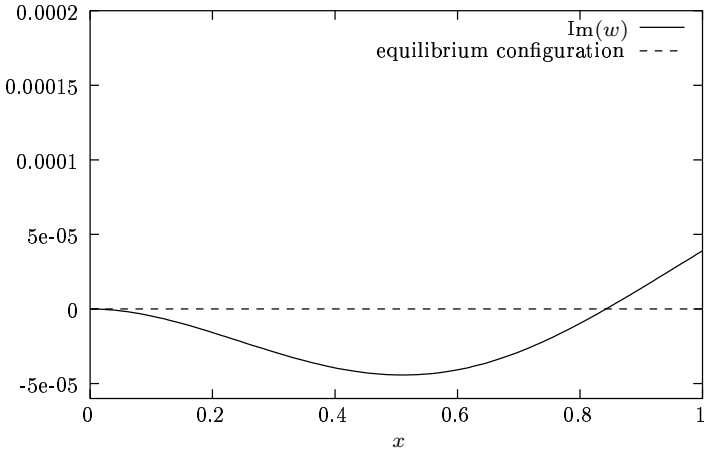

Figure 19: Imaginary part of the displacement in the unstable mode for $U = 3.070$

In figures 18 and 19 we have reported, respectively, the real and imaginary part of the unstable mode (for $U = 3.070$). Finally, in figure 20, we have reported a comparison between the frequencies of the unstable mode for each value of U. We can immediately point out the good agreement of these results.

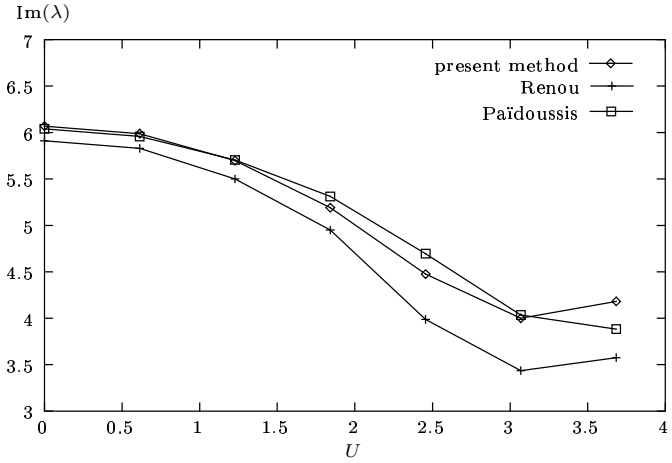

Figure 20: Frequency of the unstable mode

5.3 Wind effects on a simplified bridge deck profile

In this paragraph we deal with the aeroelastic flutter instability analysis of bluff-bodies in a steady wing. More precisely, we address the problem of flutter instabilities of prismatic cylinders with rectangular section, and chord c to thickness d ratio equal to 4, i.e. $\dfrac{c}{d} = 4$, see figure 21. This simple section has been chosen because several experimental data are available [46, 47].

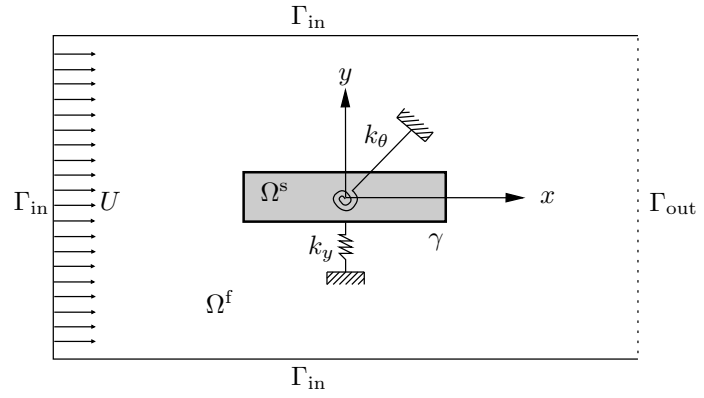

Figure 21: Fluid-structure configuration at equilibrium

As mentioned above, flutter is a self-excited oscillatory instability in which the fluid aerodynamic forces put energy into the structure and progressively increase the amplitude of the motion. It corresponds to a negative damping and occurs at any velocity above the flutter boundary. This clearly distinguishes it from vortex shedding instabilities, which are associated with a flow instability and arise when the frequency of the shed vortex in the wake coincides with the natural frequency of the structure. Moreover, vortex-excited oscillation never produce divergent amplitudes. For a more detailed description of these aeroelastic phenomena the reader can refer to [40].

In [46, 47], Washizu *et al.* investigate experimentally the aeroelastic instabilities of several prismatic cylinders with rectangular section in a heaving or in a torsional mode. We will consider here their wind tunnel free oscillation experiments. In the free oscillation method the velocity of the uniform flow U is increased step by step and, at each step, the structure is given a small initial heaving or rotating displacement and let to go. The goal here is to obtain the mean limit cyclic amplitude of the free oscillation as a function of the flow velocity.

In figures 22(a) and 22(b) we report, respectively, the free oscillation results obtained by Washizu *et al.* in [46, 47], for a rectangular cylinder of ratio 4 in a heaving and a rotating mode. In these figures, the ordinate is the amplitude of the limit cycle and the abscissa the dimensionless velocities $\frac{U}{f_y d}$ and $\frac{U}{f_\theta d}$, where f_y and f_θ stand, respectively, for the natural frequency of the structure in the heaving and torsional mode. In both figures the symbol $\diamondsuit$ indicates the resonance speed, namely, the uniform flow velocity where the frequency of the shedding vortex in the wake coincides with the natural frequency of the structure in the corresponding mode.

Figure 22(a) shows two regions of instability of which one is in the vicinity of the resonance speed. Washizu *et al.*, in [46], pointed out that if the structural damping becomes large these two regions disappear. Thus, they concluded that these two unstable regions correspond to vortex-shedding instabilities, and that no traverse flutter occurs. On the other hand, see [47], figure 22(b) indicates that vortex-excited oscillation was not observed in the free oscillation experiments, and torsional flutter can develop from a initial oscillation of small amplitude. In short, a prismatic bar of ratio 4 can not suffer flutter in a heaving mode bu this can take place in a torsional motion.

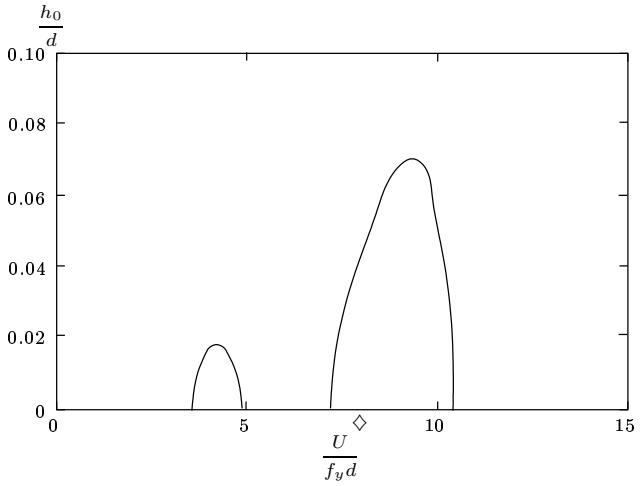

(a) Heaving mode

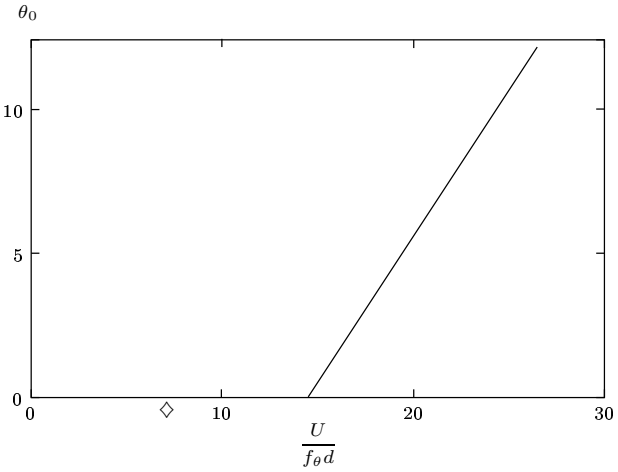

(b) Torsional mode

Figure 22: Experimental amplitude of the limit cycle, reported in [46, 47]

In this paragraph we aim to reproduce the above experimental results using the linearization-transpiration method developed in Part I [16] and the numerical analysis introduced in sections 3 and 4 of the present paper. Namely, the finite element approximation (17) combined with algorithm 1 for the leftmost eigenvalue computation.

We consider an elastically mounted rigid prismatic cylinder with rectangular section immersed in a transverse incompressible flow. We assume that the structure can only vibrate on a transverse plane perpendicular to the prism and axial effects are not considered. Hence, the problem is studied in two dimensions. As in [46, 47], we will confine our study to vertical and torsional body motions. In the sequel, Ω^{f} stands for the two-dimensional domain occupied by the fluid and Ω^{s} for the rectangular section of the prism with ratio $\frac{c}{d} = 4$, and γ denotes the fluid-structure interface.

Let us consider a uniform flow velocity $u_{\Gamma_{\mathrm{in}}} = (U, 0)^{\mathrm{T}}$ on the inlet boundary Γ_{in}, see figure 21. For low Reynolds regimes, the coupled fluid-structure system exhibits a steady equilibrium state (u_0, p_0, s_0) satisfying equations (1) and (2), i.e.

$$\begin{aligned}
\nabla u_0 u_0 - 2\nu \operatorname{div} \varepsilon(u_0) + \frac{1}{\rho}\nabla p_0, \quad & \text{in} \quad \Omega^{\mathrm{f}}, \\
\operatorname{div} u_0 = 0, \quad & \text{in} \quad \Omega^{\mathrm{f}}, \\
u_0 = u_{\Gamma_{\mathrm{in}}}, \quad & \text{on} \quad \Gamma_{\mathrm{in}}, \\
\sigma(u_0, p_0) n = 0, \quad & \text{on} \quad \Gamma_{\mathrm{out}}, \\
\mathrm{K}\, s_0 = -\int_\gamma \Phi^{\mathrm{T}} \sigma(u_0, p_0) n \, \mathrm{d}a. &
\end{aligned}$$

Here $s_0 = (y_0, \theta_0)^{\mathrm{T}} \in \mathbb{R}^2$, with y_0 the vertical displacement and θ_0 the rotation around the center of mass of the structure. In addition, the modal basis Φ is given by

$$\Phi = \left[\begin{pmatrix} 0 \\ 1 \end{pmatrix} \mid \begin{pmatrix} 0 & -1 \\ 1 & 0 \end{pmatrix} \begin{pmatrix} x \\ y \end{pmatrix} \right].$$

Remark 5.5 *Since the uniform flow is symmetric, the resultant of the fluid loads at the interface*

$$\int_\gamma \Phi^{\mathrm{T}} \sigma(u_0, p_0) n \, \mathrm{d}a = 0,$$

and then $s_0 = 0$.

The stability analysis of this equilibrium state can be carried out using the linearization-transpiration framework introduced in Part I [16]. Hence, the study of the linear stability of (u_0, p_0, s_0) reduces to the computation of the leftmost eigenvalues of problem (3), i.e.: find $\lambda \in \mathbb{C}$, $u : \Omega^{\mathrm{f}} \longrightarrow \mathbb{C}^2$, $p : \Omega^{\mathrm{f}} \longrightarrow \mathbb{C}$ and $s \in \mathbb{C}^2$, with and $(u, p, s) \neq 0$, such that

$$\begin{aligned}
\nabla u_0 u + \nabla u u_0 - 2\nu \operatorname{div} \varepsilon(u) + \frac{1}{\rho}\nabla p = \lambda u, \quad & \text{in} \quad \Omega^{\mathrm{f}}, \\
\operatorname{div} u = 0, \quad & \text{in} \quad \Omega^{\mathrm{f}}, \\
u = 0, \quad & \text{on} \quad \Gamma_{\mathrm{in}}, \\
\sigma(u,p)n = 0, \quad & \text{on} \quad \Gamma_{\mathrm{out}}, \\
u = -\lambda \Phi s - \nabla u_0 \Phi s, \quad & \text{on} \quad \gamma, \\
\lambda^2 \,\mathrm{M}\, s + \left(\mathrm{K} + \mathrm{B}^0\right) s = -\int_\gamma \Phi^{\mathrm{T}} \sigma(u,p) n \,\mathrm{d}a. &
\end{aligned} \tag{50}$$

Using the discretization scheme (17) the above eigenproblem becomes a generalized eigenvalues problem of type (23). Thus, its leftmost eigenvalues will be approximated using algorithm 1.

During our numerical computations we have fixed the following parameter values: $\rho = 1.293$ Kg/m^3, $\nu = 5 \times 10^{-5}$ m^2/s, $c = 4$ m, $d = 1$ m,

$$\mathrm{M} = \begin{pmatrix} m & 0 \\ 0 & I_\theta \end{pmatrix}, \quad \mathrm{K} = \begin{pmatrix} k_y & 0 \\ 0 & k_\theta \end{pmatrix}, \quad k_y = m w_y^2, \quad k_\theta = m w_\theta^2,$$

with $m = 100$ Kg, $I_\theta = 100$ Kg m^2 and $f_y = f_\theta = 10^{-4}$ Hz. All flow regimes are low speed, the range of Reynolds number Ud/ν was [0,80]. In such a way that, as in [46, 47], we cover a range of dimensionless velocities between 0 and 40.

The fluid domain Ω^{f} around the deck section was discretized using an unstructured mesh of 6648 triangles, see figure 23. For each value of U the steady flow (u_0, p_0) was computed using a $\mathbb{P}_2/\mathbb{P}_1$ Navier-Stokes solver (figure 24) and $\mathbb{P}_1/\mathbb{P}_1$ elements for the stability analysis. In algorithm (1) the number of requested eigenvalues was fixed to 10, the dimension of the Krylov subspace to

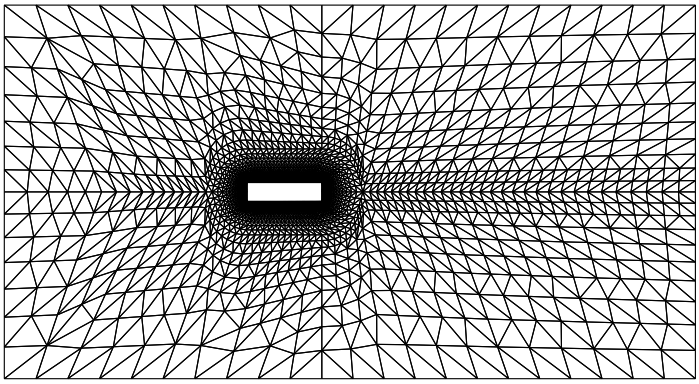

Figure 23: Triangulation of the fluid domain at equilibrium

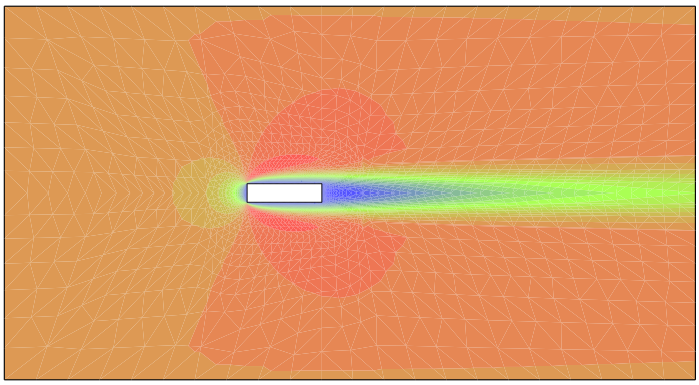

Figure 24: Iso-values of the flow $x-$velocity at equilibrium for $U = 4$ m/s

30 and the Ritz estimates tolerance to 10^{-6}. For each value of U, the mean computational time was 13 minutes on a HP Visualize 8200 workstation with 2 Cayley iterations.

First, we consider problem (50) with the rigid body oscillating in its heaving mode. In figure 25 we have plotted the damping of the system, namely, the real part of the left-most eigenvalue, as a function of the dimensionless velocity. Since $\mathrm{Re}(\lambda_1)$ only takes positive values we conclude that the reference equilibrium is stable, i.e. not flutter occurs in the range of non-dimensional velocities $[0, 45]$, as predicted by Washizu *et al.* in [46]. As mentioned above, the

vortex-shedding instability observed in [46] are associated with flow separation around the body, namely, with a flow instability. This is a unsteady phenomena that can not take place in our low speed framework. Indeed, the fluid flow is stable without interface motion (see figure 24). Therefore, vortex-shedding instabilities can not be recovered with our approach.

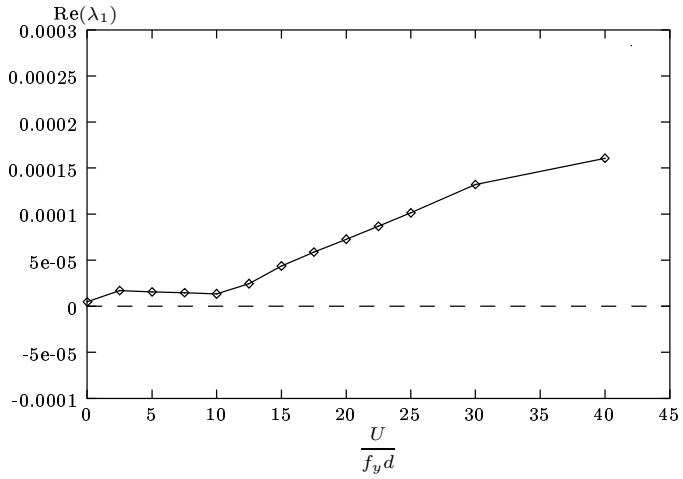

Figure 25: Real part of the leftmost eigenvalue (heaving mode)

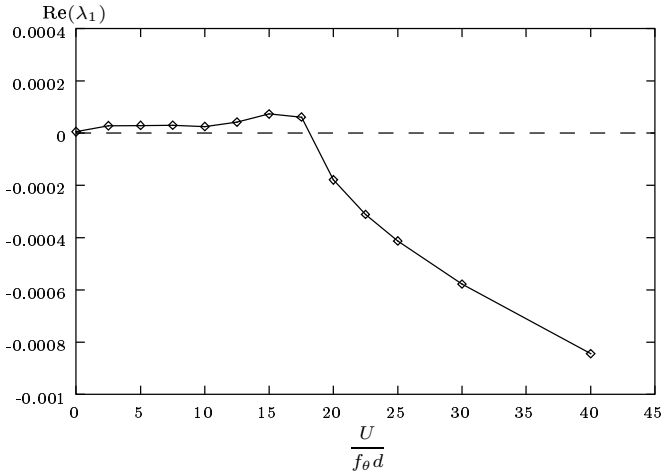

Figure 26: Real part of the leftmost eigenvalue (torsional mode)

In figure 26 we have reported the stability results for the torsional motion. These numerical results are in very good agreement with experiments in [47], see figure 22. When the velocity of the uniform flow U becomes large, the real part, $\mathrm{Re}(\lambda_1)$, of the left-most eigenvalue takes negatives values. Thus, figure 26 indicates that torsional flutter can occur in the range of dimensionless velocities [15, 45].

6 Conclusion

In this work we addressed the flutter problem of a coupled fluid-structure system involving an incompressible Newtonian fluid and a reduced structure. This was done by a linear stability approach. We used the linearization-transpiration formulation developed in Part I [16]. This allows us to reduce the stability analysis to the computation of the left-most eigenvalues of a coupled spectral problem. This coupled eigenproblem involves the linearized incompressible Navier-Stokes equations (written in a fixed domain) and those of a reduced linear structure. The coupling is realized through specific transpiration interface conditions.

We proposed a stabilized finite element method for the discretization of the fluid-structure eigenproblem. Although the numerical results pointed out the good behavior of this scheme, no error analysis was carried out in this paper. It will be a forthcoming topic of our work. The discrete formulation leads to a sparse generalized eigenvalues problem with "infinite" eigenvalues. The smallest real part eigenvalues, which are relevant for the stability analysis, were approximated by means of an iterative algorithm which combines a generalized Cayley transform and an Implicit Restarted Arnoldi Method.

Finally, we have reported three significant numerical experiments: a structure immersed in a fluid at rest, a cantilever pipe conveying a fluid flow and a rectangular bridge deck profile under wind effects. The corresponding numerical results were compared to former approaches and experimental data. The comparisons have indicated that our numerical results are very satisfactory and promising.

References

[1] G. Barrenechea and F. Valentin. An unusual stabilized finite element method for a generalized Stokes problem. *Numer. Math.*, 2002. To appear.

[2] A.N. Brooks and T.J.R. Hughes. Streamline upwind/Petrov-Galerkin formulations for convection dominated flows with particular emphasis on the incompressible Navier-Stokes equations. *Comput. Methods Appl. Mech. Engrg.*, 32(1-3):199–259, 1982.

[3] F. Chatelin. *Valeurs propres de Matrices.* Masson, Paris, 1988.

[4] F. Chatelin and D. Ho. Arnoldi-Tchebychev procedure for large scale nonsymmetric matrices. *Math. Modeling and Num. Analysis*, 24:53–65, 1990.

[5] P.G. Ciarlet. *The finite element method for elliptic problems.* North-Holland, Amsterdam, 1978.

[6] K.A. Cliffe, T.J. Garratt, and A. Spence. Eigenvalues of block matrices arising from problems in fluid mechanics. *SIAM J. Matrix Anal. Appl.*, 15(4):1310–1318, 1994.

[7] C. Conca and M. Durán. A numerical study of a spectral problem in solid-fluid type structures. *Numer. Methods Partial Differential Equations*, 11(4):423–444, 1995.

[8] C. Conca, M. Durán, and J. Planchard. A quadratic eigenvalue problem involving Stokes equations. *Comput. Methods Appl. Mech. Engrg.*, 100(3):295–313, 1992.

[9] C. Conca, J. Planchard, B. Thomas, and M. Vanninatahn. *Problèmes mathématiques en couplage fluide-structure.* Eyrolles, Paris, 1994.

[10] R. Dautray and J.L. Lions. *Mathematical analysis and numerical methods for science and technology. Vol. 2.* Springer-Verlag, Berlin, 1988.

[11] T.A. Davis and I.S. Duff. A combined unifrontal/multifrontal method for unsymmetric sparse matrices. Technical Report 20, CISE, University of Florida, 1999.

[12] Y. Ding and M. Kawahara. Linear stability of incompressible flow using a mixed finite element method. *J. Comput. Phys.*, 139(2):243–273, 1998.

[13] Y. Ding and M. Kawahara. Three-dimensional linear stability analysis of incompressible viscous flows using the finite element method. *Internat. J. Numer. Methods Fluids*, 31(2):451–479, 1999.

[14] T. Fanion, M.A. Fernández, and P. Le Tallec. Deriving adequate formulations for fluid-structure interactions problems: from ALE to transpiration. *Rév. Européenne Élém. Finis*, 9(6-7):681–708, 2000.

[15] M.A. Fernández. *Modéles simplifiés d'interaction fluide-structure.* PhD thesis, Université de Paris IX, 2001.

[16] M.A. Fernández and P. Le Tallec. Linear stability analysis in fluid-structure interaction with transpiration. Part I: formulation and mathematical analysis. Submited, 2002.

[17] L. P. Franca and F. Valentin. On an improved unusual stabilized finite element method for the advective-reactive-diffusive equation. *Comput. Methods Appl. Mech. Engrg.*, 190(13-14):1785–1800, 2000.

[18] J.N. Franklin. *Matrix theory.* Prentice-Hall, New Jersey, 1968.

[19] T.J. Garrat. *The numerical detection of Hopf bifurcations in large systems arising in fluids mechanics.* PhD thesis, University of Bath, 1991.

[20] T. J. Garratt, G. Moore, and A. Spence. Two methods for the numerical detection of Hopf bifurcations. In *Bifurcation and chaos: analysis, algorithms, applications (Würzburg, 1990)*, pages 129–133. Birkhäuser, Basel, 1991.

[21] T.J. Garratt, G. Moore, and A. Spence. A generalised Cayley transform for the numerical detection of Hopf bifurcations in large systems. In

Contributions in numerical mathematics, pages 177–195. World Sci., River Edge, 1993.

[22] A. Georgescu. *Hydrodynamic stability theory.* Martinus Nijhoff, Dordrecht, 1985.

[23] V. Girault and P.A. Raviart. *Finite element methods for Navier-Stokes equations.* Springer-Verlag, Berlin, 1986.

[24] G. Hauke and A. García-Olivares. Variational subgrid scale formulations for the advection-diffusion-reaction equation. *Comput. Methods Appl. Mech. Engrg.*, 190(51-52):6847–6865, 2001.

[25] T.J.R. Hughes and A. Brooks. A multidimensional upwind scheme with no crosswind diffusion. In *Finite element methods for convection dominated flows (Papers, Winter Ann. Meeting Amer. Soc. Mech. Engrs., New York, 1979)*, pages 19–35. Amer. Soc. Mech. Engrs. (ASME), New York, 1979.

[26] T.J.R. Hughes, L.P. Franca, and M. Balestra. A new finite element formulation for computational fluid dynamics. V. Circumventing the Babuška-Brezzi condition: a stable Petrov-Galerkin formulation of the Stokes problem accommodating equal-order interpolations. *Comput. Methods Appl. Mech. Engrg.*, 59(1):85–99, 1986.

[27] P. Le Tallec. *Introduction à la dynamique des structures.* Les Cours de l'École polytechnique. Ellipses, Paris, 2000.

[28] P. Le Tallec and J. Mouro. Fluid structure interaction with large structural displacements. *Comput. Methods Appl. Mech. Engrg.*, 190(24-25):3039–3067, 2001.

[29] R.B. Lehoucq and A.G. Salinger. Large-scale eigenvalue calculations for stability analysis of steady flows on massively parallel computers. *Internat. J. Numer. Methods Fluids*, 36(3):309–327, 2001.

[30] R.B. Lehoucq and J.A. Scott. Implicitly restarted Arnoldi methods and eigenvalues of the discretized Navier-Stokes equations. Technical Report 2712J, Sandia National Laboratories, 1997.

[31] R.B. Lehoucq and D.C. Sorensen. Deflation techniques for an implicitly restarted Arnoldi iteration. *SIAM J. Matrix Anal. Appl.*, 17(4):789–821, 1996.

[32] R.B. Lehoucq, D.C. Sorensen, and C. Yang. *ARPACK users' guide. Solution of large-scale eigenvalue problems with implicitly restarted Arnoldi methods.* Society for Industrial and Applied Mathematics (SIAM), Philadelphia, 1998.

[33] M. Lesoinne, M. Sarkis, U. Hetmaniuk, and C. Farhat. A linearized method for the frequency analysis of three-dimensional fluid/structure interaction problems in all flow regimes. *Comput. Methods Appl. Mech. Engrg.*, 190:3121–3146, 2001.

[34] K. Meerbergen and A. Spence. Implicitly restarted Arnoldi with purification for the shift-invert transformation. *Math. Comp.*, 66(218):667–689, 1997.

[35] M.P. Païdoussis. *Fluid-structure interactions: slender structures and axial flow*, volume 1. Academic Press, London, 1998.

[36] S. Piperno and P.E. Bournet. Numerical simulations of wind effects on flexible civil engineering structures. *Rev. Eur. Élém. Finis*, 8(5-6):659–687, 2001.

[37] J.Y. Renou. *Une méthode eulérienne pour le calcul de forces fluide-élastiques.* PhD thesis, Université de Paris VI, 1998.

[38] Y. Saad. Numerical solution of large nonsymmetric eigenvalue problems. *Comput. Phys. Comm.*, 53(1-3):71–90, 1989.

[39] Y. Saad. *Numerical methods for large eigenvalue problems.* Halsted Press-John Wiley & Sons, New York, 1992.

[40] E. Simiu and R.H. Scanlan. *Wind effects on structures. Fundamentals and Applications to Design.* John Wiley & Sons, Inc., New York, 1996.

[41] D.C. Sorensen. Implicit application of polynomial filters in a k-step Arnoldi method. *SIAM J. Matrix Anal. Appl.*, 13(1):357–385, 1992.

[42] G.V. Stewart. *Introduction to matrix computations.* Academic Press, New York, 1973.

[43] L. Tobiska and R. Verfürth. Analysis of a streamline diffusion finite element method for the Stokes and Navier-Stokes equations. *SIAM J. Numer. Anal.*, 33(1):107–127, 1996.

[44] S. Turek. *Efficient solvers for incompressible flow problems.* Springer-Verlag, Berlin, 1999.

[45] F. Valentin. *Nouvelles conditions aux limites équivalentes pour des interfaces rugueuses en mécanique des fluides : développement, analyse et mise en oeuvre numérique.* PhD thesis, Université de Paris VI, 1998.

[46] K. Washizu, A. Ohya, Y. Otsuki, and K. Fujii. Aeroelastic instability of rectangular cylinders in a heaving mode. *J. Sound Vib.*, 59(2):195–210, 1978.

[47] K. Washizu, A. Ohya, Y. Otsuki, and K. Fujii. Aeroelastic instability of rectangular cylinders in a torsional mode due to a transverse wind. *J. Sound Vib.*, 72(4):507–521, 1980.

Contents

Unité de recherche INRIA Rocquencourt
Domaine de Voluceau - Rocquencourt - BP 105 - 78153 Le Chesnay Cedex (France)

Unité de recherche INRIA Lorraine : LORIA, Technopôle de Nancy-Brabois - Campus scientifique
615, rue du Jardin Botanique - BP 101 - 54602 Villers-lès-Nancy Cedex (France)
Unité de recherche INRIA Rennes : IRISA, Campus universitaire de Beaulieu - 35042 Rennes Cedex (France)
Unité de recherche INRIA Rhône-Alpes : 655, avenue de l'Europe - 38330 Montbonnot-St-Martin (France)
Unité de recherche INRIA Sophia Antipolis : 2004, route des Lucioles - BP 93 - 06902 Sophia Antipolis Cedex (France)

Éditeur
INRIA - Domaine de Voluceau - Rocquencourt, BP 105 - 78153 Le Chesnay Cedex (France)
http://www.inria.fr
ISSN 0249-6399